THE ASTROPHYSICAL JOURNAL, 450:302–317, 1995 September 1

THE CHEMICAL COMPOSITION OF RED GIANTS. IV. THE NEUTRON DENSITY AT THE *s*-PROCESS SITE

DAVID L. LAMBERT,[1] VERNE V. SMITH,[1] MAURIZIO BUSSO,[2] ROBERTO GALLINO,[3] AND OSCAR STRANIERO[4]
Received 1995 January 11; accepted 1995 March 8

ABSTRACT

Rubidium abundances are determined from the Rb I 7800 Å line via synthetic spectra for a sample of M, MS, and S giants. The Rb abundance increases with increasing *s*-process enrichment. A ratio Rb/Sr $\simeq$ 0.05 is derived for the *s*-processed material from the He-burning shell. Thanks to the branch in the *s*-process path at ^{85}Kr the Rb/Sr ratio may be used to determine the neutron density at the time of *s*-processing. The derived ratio is consistent with predicted neutron densities for operation of the *s*-process during the interpulse intervals in low-mass asymptotic giant branch (AGB) stars but clearly inconsistent with much higher neutron densities predicted for the running of the *s*-process in the He-shell thermal pulses of intermediate mass AGB stars and probably also of low-mass AGB stars.

Zirconium isotopic abundances are determined from ZrO bandheads near 6925 Å via synthetic spectra for a sample of S stars. No evidence is found for the isotope ^{96}Zr whose synthesis is controlled by the branch in the *s*-process path at ^{95}Zr. This observation shows that the observed stars are not intermediate mass stars with massive ($M_C \gtrsim 1\ M_\odot$) cores. The absence of ^{96}Zr sets an upper limit on the neutron density at the *s*-process site which is higher than and, therefore, consistent with the limit set by the Rb abundances in related stars.

Subject headings: nuclear reactions, nucleosynthesis, abundances — stars: abundances — stars: late-type

1. INTRODUCTION

Merrill's (1952) discovery of technetium in the spectra of S stars showed that these stars must currently be synthesizing Tc and other elements. Synthesis occurs by successive captures of neutrons such that the heavy elements are synthesized from abundant Fe-peak (seed) nuclei. Synthesis occurs at a low neutron density such that the first unstable neutron-rich isotope of an element, in general, decays rather than capturing another neutron. Synthesis at these low neutron densities is universally referred to as "the *s*-process" (Burbidge et al. 1957).

In previous papers (Smith & Lambert 1985, 1986, 1990), we have investigated the elemental abundances of "*s*-process" elements in MS and S stars. MS/S stars containing Tc are asymptotic giant branch (hereafter, AGB) stars in which the *s*-process operates in the He shell. Operation of the *s*-process was until recently identified with the He-shell flash or thermal pulses experienced intermittently by the AGB stars. Straniero et al. (1995a, b) have, however, shown that neutrons may be released prior to the thermal pulse at a time when the He shell is in a radiative condition rather than in the convective condition attained in the thermal pulse. These calculations done for a 3 $M_\odot$ star have yet to be extended to other masses.

Many MS/S stars with unmistakable overabundances of "*s*-process" elements lack Tc in their atmospheres. Brown et al. (1990) and Jorissen et al. (1993) show conclusively that these MS/S stars belong overwhelmingly to binary systems in which the companion is probably a white dwarf. As first suggested by Iben & Renzini (1983), the MS/S stars without Tc may be identified as close relatives (most probably direct descendants) of the barium giants of earlier spectral type (G and K) and lower luminosity. In these systems, the *s*-process operated in the He shell of an AGB star (now the white dwarf) which, by mass transfer, converted its companion to the *s*-process enriched star that we now observe as a MS/S giant. This giant may be on the red giant branch prior to the He-core flash or on the AGB but at luminosities too low for ignition of the He shell. Of course, the MS/S stars without Tc may evolve to burn He during pulses and, then, Tc may again be present in a star's atmosphere. A consideration of the relative lifetimes of cool giants prior to and following the onset of the thermal pulses suggests that evolved barium giants with fresh Tc should be rare. In this paper, we refer to the MS/S stars with Tc as "intrinsic" AGB stars and to the MS/S stars without Tc as "extrinsic" AGB stars. The composition of the extrinsic stars is presumed to be a mix of a portion of an AGB (intrinsic) star's envelope with the envelope of the mass gaining star.

Our analyses of the elemental abundances of intrinsic and extrinsic MS/S stars shows that, in our approximately magnitude-limited sample of Galactic stars, the *s*-process site provides a neutron exposure similar to that experienced by solar system material (Smith & Lambert 1990). The investigated elements from roughly Sr to Nd constitute what is called the "main" component in the *s*-process. The degree of overabundance of these elements is a measure of the ratio of the mass of material from the *s*-process site (M_s) to the mass of the unprocessed envelope (M_{env}): $M_s/M_{env} \sim 0.1\%$–0.3% for the typical star with $M_s/M_{env} \sim 1\%$ in one extreme case (TV Aur.) The mean neutron exposure increases with decreasing metallicity as predicted by Clayton (1988) and observed by Vanture (1992), Luck & Bond (1991), and North, Berthet, & Lanz (1994) for CH or Barium giants and dwarfs—see discussion by Busso et al. (1995).

In this paper, we probe deeper into the operation of the *s*-process in the He shell of AGB stars: we examine the neutron density. In the limit that the neutron density, $N(n)$, tends to

[1] Department of Astronomy, University of Texas, Austin, Texas 78712.
[2] Osservatorio Astronomico di Torino, Strada Osservatorio 20, I-10025 Pino Torinese, Italy.
[3] Istituto di Fisica Generale, Università di Torino, Via P. Giura 1, I-10125, Torino, Italy.
[4] Osservatorio di Collurania, I-64100 Teramo, Italy.

zero, the *s*-process takes a unique path along the valley of stability because all unstable nuclei decay rather than capture a neutron. At the neutron densities expected in an AGB's He shell, a competition may arise at certain unstable nuclei between decay and neutron capture. These nuclei serve as branch points in the *s*-process path. For each branch point, there is a critical value of the neutron density $N(n)_c$: if $N(n) \ll N(n)_c$, the unstable nuclide at the branch decays, but if $N(n) \gg N(n)_c$, the unstable nuclide captures a neutron. The magnitude of $N(n)_c$ is set by the ratio of the unstable nuclide's rate of decay (usually β-decay) and its neutron capture cross section. The switch of a branch from the $N(n) \ll N(n)_c$ to the $N(n) \gg N(n)_c$ path occurs over a factor of about 1000 in $N(n)$. The two possible paths that are open for $N(n) \sim N(n)_c$ reunite after a few neutron captures. For nuclides on the alternative paths, their abundance obviously depends on the neutron density and may also depend on other physical characteristics of the *s*-process site such as temperature and the variation of neutron flux with time. Käppeler, Beer, & Wisshak (1989) provide a thorough discussion of the several branches that may be analyzed using the accurate and comprehensive nuclidic abundances available from carbonaceous chondrites.

In this paper, we investigate the two branches that may provide information on the neutron density in the He-burning shell of AGB stars: the branch at ^{85}Kr determines the abundance of Rb relative to its neighbors Sr and Y; the branch at ^{95}Zr controls the synthesis of the stable isotope ^{96}Zr. The Rb abundance is determined from observations of the Rb I 7800 Å resonance line. The isotopic abundances of Zr are estimated from spectra of ZrO bandheads near 6930 Å.

2. OBSERVATIONS

2.1. *The* Rb I 7800 Å *Line*

Rubidium is of such low abundance that it must be sought through its resonance lines at 7800 Å and 7947 Å. In the case of the MS/S stars, these lines fall within a region rich in molecular lines with TiO being the leading contributor. Preliminary observations showed that the 7947 Å line is too badly blended to warrant analysis. All of the estimates below are based on comparisons of observed and synthetic spectra for the 7800 Å line.

In spectra of normal red giants, the 7800 Å Rb I line is a useful abundance indicator over a restricted range of effective temperature. If the giant is warmer than about 4000 K, the TiO lines are very weak or absent, but the weak Rb I line is badly blended with a stronger Si I line. Cooler than $T_{\rm eff} \approx 4000$ K, the Rb I line and the TiO lines strengthen, but the Rb I line proves to be distinguishable from adjacent and blending TiO lines for stars in the temperature range $4000 \gtrsim T_{\rm eff} \gtrsim 3300$ K unless the C/O ratio is near unity: comparison of the spectra of a MS/S star and a normal M star of similar temperature shows that the Rb I line is stronger in the former. In cool S stars such as TV Aur (and the SC stars), the higher C/O abundance ratio leads to weaker TiO lines and the Rb I line is a prominent line set among a background of much weaker lines.

At $T_{\rm eff} \lesssim 3300$ K, Rb I is indistinguishable as a line and the residual flux in the core of the Rb I/TiO blend is very similar to the flux in the cores of all other TiO features; this flux increases slowly over the bandpass from 7760 to 7850 Å. The fact that the residual fluxes are approximately constant suggests that these line cores are formed at the top of the photosphere where the temperature gradient is very shallow. Since the Rb I/TiO blend and the TiO features are at a common depth, the former is, by definition, "saturated" and insensitive to the Rb abundance. We made no attempt to extract the Rb abundance for these cool normal giants. The two cool MS/S stars with strong TiO lines that were observed—RS Cnc and Y Lyn—show a line apparently not present in the spectra of warmer stars. In the spectrum of Y Lyn, this additional line is deeper (lower residual flux) than the series of adjacent TiO features. This new line may be the circumstellar Rb I line formed in a slowly expanding shell. If identified as Rb I, the expansion velocity is 10–20 km s^{-1}, a typical value. Circumstellar lines of Rb I at 7800 and 7947 Å were detected first by Tsuji (1971) in spectra of the long-period variables (LPV) R And and R Cyg. Our spectra of the Li-rich LPV T Sgr also show a circumstellar Rb I line.

Spectra around 7800 Å were obtained with the coudé spectrometer of the McDonald Observatory's 2.7 m reflector. A majority of the spectra were recorded with either a Reticon array or a Texas Instruments CCD at a resolution of 0.2 Å over a bandpass of 110 Å (Reticon) or 50 Å (CCD). Stars for which a Rb abundance was determinable are listed in Table 1.

2.2. ZrO *Bandheads*

Isotopic Zr abundances are not discernible from even high resolution spectra of Zr atomic lines but the ZrO band systems provide possibly multiple opportunities to extract the isotopic abundances. Pioneering work on the isotopic Zr abundances was done by Schadee & Davis (1968) and Peery & Beebe (1970) on the ($A\ ^3\Phi - X'\ ^3\Delta$) γ-system's 0–0 band near 6370 Å. Such an analysis is difficult because lines of the several isotopes are intermingled. (Clegg, Lambert, & Bell 1979 successfully analyzed an analogous band of TiO to extract isotopic Ti abundances.) Zook (1978, 1985) took advantage of the larger isotopic shifts provided by the $B\ ^1\Pi - X\ ^1\Sigma^+$ 0–1 band near 6931 Å, where there is a progression of bandheads from ^{96}ZrO at the shortest wavelength to ^{90}ZrO at about 2 Å from the ^{96}ZrO head. Our observations at 6925 Å were designed to cover both the $B-X$ 0–1 bandhead and the 1–2 bandhead of the γ-system at 6923 Å, where the isotopic bandheads are similarly organized: ^{96}ZrO at 6921.1 Å through to ^{90}ZrO at 6923.4 Å.

Two sets of observations comprise the ZrO data: spectra taken at "high resolution," and some spectra taken at "moderate resolution." The high-resolution spectra were taken with the McDonald Observatory's 2.7 m reflector and coudé spectrometer with an echelle grating and an order-sorting interference filter. The dector was a 1872 element Reticon and the spectra were centered near 6920 Å. The scale at the Reticon was 0.015 Å pixel^{-1} and the slit opening corresponded to 5 pixels at the detector yielding a resolution of 0.075 Å, or $R = 92{,}000$ at 6910 Å. The moderate-resolution spectra were also taken with the McDonald 2.7 m and coudé spectrometer, but with a plane grating used in first order providing a scale of 0.064 Å pixel^{-1} on a TI CCD detector. A slit opening of 3 pixels at the CCD was used yielding a resolution of 0.19 Å, or $R = 36{,}000$ at 6920 Å. Both sets of spectra contained the ZrO γ 1–2 and the $B-X$ 0–1 bandheads.

Hot, rapidly rotating stars were observed on each night that program stars were observed, in order to ratio out the telluric O_2 and H_2O lines found in this region. All stars observed in which strong ZrO was found are variable S stars and in Figure 1 we show an example of an S star observed on two dates, R Gem, illustrating the $B-X$ 0–1 bandhead. In these echelle

TABLE 1

RUBIDIUM AND *s*-PROCESS ABUNDANCES

	Star	Sp. Type	$T_{\rm eff}$ [K]	$\log g$ [cm s^{-2}]	$\left[\frac{\rm M}{\rm H}\right]$	$\left[\frac{s}{\rm M}\right]$	$\left[\frac{\rm Rb}{\rm M}\right]$	Tc
HR 337	β And	M0IIIa	3800	1.6	−0.1	+0.1	−0.3	no
HR 363		S3$^+$/2$^-$	3600	1.2	−0.1	+0.5	+0.1	no
HR 921	ρ Per	M4II	3500	0.8	−0.1	−0.2	−0.1	no
HR 1105		S3.5/2	3600	1.2	−0.1	+0.8	+0.1	no
HR 1457	α Tau	K5III	3850	1.5	0.0	0.0	−0.2	no
HR 1556	o^1 Ori	S3.5/1$^-$	3450	0.8	−0.1	+0.9	+0.2	yes
BD +48°1187	TV Aur	S5/6$^-$	3200	0.0	+0.1	+1.4	+0.6	yes
HD 35155		S3/2	3550	0.8	−0.5	+0.7	+0.2	no
HR 2508		M1Ib–IIa	3600	0.7	+0.1	0.0	−0.3	yes
HD 49368		S3/2	3700	1.0	−0.2	+0.7	+0.1	no
HR 2990	β Gem	K0IIIb	4800	2.8	0.0	0.0	0.0	no
HD 64332	NQ Pup	S4.5/2$^-$	3500	0.5	−0.3	+0.6	+0.2	yes
HR 4088	44 Leo	M3IIIabs	3700	1.4	0.0	0.0	−0.2	no
HR 4483	ω Vir	M4III	3450	0.8	0.0	−0.1	−0.2	no
HR 4517	ν Vir	M1IIIab	3750	1.5	0.0	+0.1	−0.2	no
HR 4910	δ Vir	M3III	3650	1.5	+0.1	−0.1	−0.2	no
HR 5226	10 Dra	M3.5III	3650	1.5	0.0	−0.3	−0.2	no
HR 5299		M4III	3500	0.8	−0.1	+0.3	−0.1	no
HD 172804		S5/6$^-$	3400	0.3	−0.1	+0.9	+0.6	yes
HR 7442		M4.5IIIas	3500	0.8	0.0	−0.1	−0.1	no
HR 8062		S4/1	3450	0.7	+0.1	+0.3	−0.2	yes
HR 8714		S4$^+$/1$^+$	3500	0.9	−0.1	+0.5	0.0	yes
HR 8775	β Peg	M2.5II–III	3600	1.2	−0.1	+0.1	−0.3	no

spectra, the various Zr isotopes are easily visible. It is clear that the relative shape of the isotopic bands does not change from one phase of the star to the other. At the lower resolution of the grating spectra, the ZrO isotopic bands are largely blended, and are not clearly visible. A S/N ratio of not less than 100 was generally obtained in the continuum of the ratioed echelle and grating spectra. Stars considered here for analysis are listed in Table 2.

3. THE RUBIDIUM ABUNDANCES

3.1. *Basic Data*

In spectra of the cool oxygen-rich giants that comprise our list of stars, the 7800 Å Rb I resonance line is within the $\Delta v = -1$ sequence of the TiO γ system: the TiO lines dominate the stellar spectrum and several TiO lines are blended with the Rb I line. The Rb abundance is extracted using synthetic spectra. Two somewhat distinct contributions from TiO are considered: (1) all known TiO lines are included in the line list (2) a quasi-continuous opacity is added to the continuous absorption coefficient provided by (primarily) the H^- ion. The quasi-continuous TiO opacity is attributed to a thicket of overlapping and mostly weak TiO lines. We recall that such a contribution to the opacity was required in an analysis (Luck & Lambert 1982) of Fe I and other atomic lines around the Li I 6707 Å feature: when the quasi-continuous opacity was omitted, these atomic lines yielded unreasonably low elemental abundances.

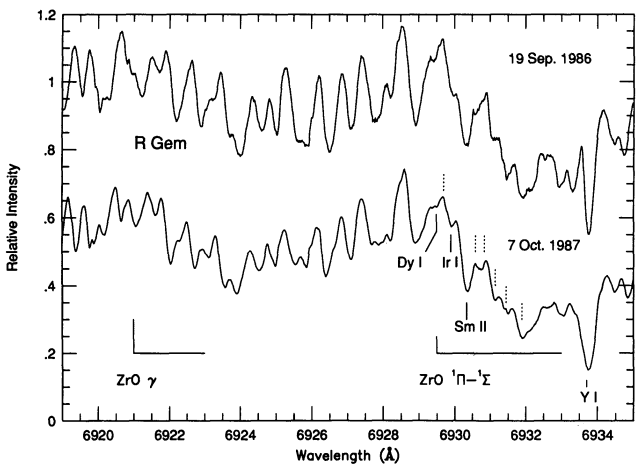

FIG. 1.—$B-X$ 0–1 ZrO bandhead in the spectrum of R Gem taken at two phases. Note the general similarity in the shapes, positions, and depths of the various absorption features. The ZrO bandheads are indicated. The dashed lines indicate the position of the $B-X$ 0–1 ZrO isotopic bandheads with ^{90}ZrO occurring at the longest wavelength, followed by ^{91}ZrO, ^{92}ZrO, ^{93}ZrO, ^{94}ZrO, and the expected position of ^{96}ZrO between the Dy I and Ir I lines.

J. G. Phillips & S. P. Davis (1974, private communication) provided a line list of ^{48}TiO lines near 7800 Å. The listed lines are those measured and classified off laboratory spectra. Lines from the four less abundant stable Ti isotopes (^{46}Ti, ^{47}Ti, ^{49}Ti, and ^{50}Ti) were added to the line list with wavelengths kindly provided by Professor Roger A. Bell. Throughout the analyses, we assumed that the isotopic abundance ratios ^{i}Ti/^{48}Ti were identical to their solar system values (Anders & Grevesse 1989). This assumption is supported by the isotopic abundances estimated by Clegg et al. (1979) for a sample of M, MS, and S stars that included several of the stars analyzed here. The precise isotopic abundance ratios are, however, unimportant because the line density from the four less abundant isotopes is so high that individual lines are not resolved and the principal effect of the many weak lines is to reduce slightly the local continuum that is defined by the "high" points in the spectrum. The lines from Ti^{17}O and Ti^{18}O may be safely omitted. No attempt has been made to predict additional TiO lines using the known molecular constants.

Excitation energies for TiO were computed from the molecular constants (Phillips 1973). TiO densities were computed using the dissociation energy [D_0(TiO) = 6.92 ± 0.10 eV]

TABLE 2

ISOTOPIC ZIRCONIUM ABUNDANCES

Star	Sp. Type	Mode[a]	System i =	^{i}Zr/Zr (per cent) 90	91	92	93	94	96
R And	S6,6e	E	B–X	32	18	14	7	14	< 5
		E	γ	40	12	21	4	22	< 2
		G	B–X	36	11	14	7	30	< 2
BI And	S8,8	G	B–X	48	14	15	4	16	< 3
T Cam	S4,7e	E	B–X	34	18	13	11	19	< 2
		E	γ	38	15	17	6	20	< 2
S Cas	S4,6e	G	B–X	49	11	16	3	16	< 5
U Cas	S5,5e	G	B–X	44	10	20	9	14	< 3
AD Cyg	S5,8	E	B–X	30	16	16	14	23	< 2
		E	γ	35	15	20	7	21	< 2
R Gem	S3,9e	E	B–X	35	20	13	3	25	< 4

[a] E ≡ echelle and G ≡ grating (see text).

recommended by Pedley & Marshall (1983). The equilibrium constant, K_p(TiO), was taken from Tsuji (1973) and corrected for the adopted D_0. Partial pressures of Ti and O were computed from the usual set of coupled equations describing the ionization of Ti and the molecular dissociation equilibrium to which the leading contributors are TiO and CO.

Oscillator strengths (gf-values) for the TiO γ-system (triplet) lines were estimted from the band f-value measured by Davis, Littleton, & Phillips (1986) who made laboratory measurements of absorption spectra of TiO singlet and triplet systems to obtain relative f-values and placed these on an absolute scale using a measurement of the radiative lifetime of the $c^1\Phi$ state (Feinberg & Davis 1977). (Lifetimes of excited triplet states were measured recently by Doverstål & Weijnitz 1992.) For the 1–0 γ-band this method gives $f_{10} = 0.039 \pm 0.007$. To calculate $f_{v'v''}$ for the γ-system's $\Delta v = -1$ sequence, we assume that the electronic transition moment (R_e^2) is independent of the internuclear separation (r) over the range in r spanned by the 1–0 and the $\Delta v = -1$ bands: i.e.,

$$f_{v'v''} = \frac{q_{v'v''}\,\sigma_{v'v''}}{q_{10}\,\sigma_{10}} f_{10} ,$$

where the Franck-Condon factors $q_{v'v''}$ are given by Bell et al. (1979) and the band frequencies $\sigma_{v'v''}$ are computed from the molecular constants. This procedure gives the band f-values: $f_{01} = 0.034, f_{12} = 0.048$, and $f_{23} = 0.048$.

The gf-values of individual TiO lines are given by the standard expression:

$$gf = \frac{\sigma}{\sigma_{v'v''}} S_{J'J''} f_{v'v''} ,$$

where the Hönl-London factors $S_{J'J''}$ are computed using a standard code (Whiting 1972) and are normalized (Larson 1983) such that

$$\sum_{J'} S_{J'J''} = 6(2J'' + 1) .$$

A majority of the TiO lines come from high rotational states and, hence, the (rotationless) Franck-Condon factors are not strictly appropriate. The predicted corrections to $q_{v'v''}$ to obtain $q_{v'J'v''J''}$ are of the order of 10% or less according to the Bell et al. (1979) computations that are based on the assumption that R_e^2 is independent of the internuclear separation. Since the corrections are smaller than the uncertainty in the gf-values resulting from the calibrating band f-value (f_{10}) and are dependent on the unknown form of R_e^2, we have ignored the effect of the vibration-rotation interaction on the Franck-Condon factors; i.e., $q_{v'J'v''J''} = q_{v'v''}$ is assumed.

Atomic lines in an approximately 100 Å interval around the Rb I line were included in our synthesis. The gf-values of many of the most prominent atomic lines were estimated from their equivalent widths in the solar spectrum, a standard solar photospheric model (Holweger & Müller 1974), and the solar elemental abundances (Anders & Grevesse 1989). When the solar line was weak or undetectable, the gf-value was estimated from the line's equivalent width in the spectrum of a K giant (β Gem or α Tau). A few CN lines (Davis & Phillips 1963) complete the line list—see Smith & Lambert (1985, 1986, 1990) for the choice of basic data [D_0(CN), $f_{v'v''}$].

The Rb line is represented correctly by the hyperfine components of both the isotopes ^{85}Rb and ^{87}Rb—see Lambert & Mallia (1968) for the gf-values, etc. The isotopic ratio was assumed to be the solar system value: ^{85}Rb/^{87}Rb = 2.6 (Anders & Grevesse 1989). Since ^{87}Rb is unstable ($\tau_{1/2} = 5 \times 10^{11}$ yr), the isotopic ratio ^{85}Rb/^{87}Rb increases with time: the current value for the solar system is reduced by only about 7% when it is extrapolated back to the origin of the solar system.

3.2. *Spectrum Synthesis and the* Rb *Abundance*

Synthetic spectra were computed using a version of the computer code written by Sneden (1973). LTE is assumed. The model atmospheres adopted were those used earlier by us (Smith & Lambert 1990).

Attempts to fit a synthetic spectrum to the 100 Å interval containing the 7800 Å Rb I line require an external constraint in order to achieve a fit that has a semblance of uniqueness. Factors to be considered in matching a synthetic spectrum to an observed spectrum include the inadequacy of the basic data for the TiO molecule, the location of the continuum, the magnitude of the quasi-continuous opacity from the TiO molecule, and the model atmosphere. Our principal constraint on the synthetic spectra is that the metal lines in the interval give abundances close to those derived earlier (Smith & Lambert 1990) from atomic lines in windows between molecular bands. Then, the Rb abundance from the best fit to the 7800 Å line is quoted as a ratio [Rb/M], where M denotes the metal (Ti, Fe, Ni) abundance derived from the 7800 Å analysis. Experiments

show that [Rb/M] is insensitive to the fit to the metal lines: synthetic spectra yielding M abundances differing by quite large amounts give quite similar [Rb/M]-values.[5]

As a first step toward the analysis of the stars which are severely blanketed by TiO lines, we undertook the analysis of α Tau, where TiO lines are weak and the continuum may be plausibly identified with the many high points in the 100 Å bandpass. Comparison of synthetic and observed spectra quickly showed a problem: the picket fence of weak TiO lines is reproduced well for an abundance log ϵ(Ti) = 4.35 or [Ti/H] = −0.6. This Ti underabundance is at odds with the metallicity obtained from atomic lines: 11 atomic lines from 7745–7850 Å give a mean [M/H] = -0.1 ± 0.1. The latter value is in good agreement with the metallicity obtained previously by Kovács (1983) who gave [Ti/H] $\simeq -0.1 \pm 0.3$ from Ti I and Ti II lines. The stronger γ 0–0 TiO lines near 7060 Å were observed earlier (Luck & Lambert 1977) and our synthetic spectra for these lines confirm the low Ti abundance. We have explored two explanations for the low Ti abundance provided by the fit to the TiO lines.

In the first of these explanations, we examined the leading sources of uncertainty to assess the likely total uncertainty. These sources and their associated uncertainty include:

1. The equilibrium constant: replacement of our K_p by that computed by Tatum & Sauval (1984) increases the Ti abundance by 0.1 dex.
2. The dissociation energy: the quoted uncertainty of ± 0.10 eV translates to an abundance uncertainty of ∓ 0.15 dex.
3. The C and O abundances: the number density of TiO molecules is determined in part by the partial pressure of free oxygen atoms that is proportional to the difference between the O and C abundances. If these abundances are taken to the appropriate limits of their uncertainty (Smith & Lambert 1990), the required Ti abundance may be increased by 0.2 dex.
4. The TiO f-values: the quoted uncertainty for the f_{10} band is $\pm 20\%$ and $\pm 30\%$ (or ± 0.1 dex) seems appropriate for our high-J lines from bands that belong to a different sequence.
5. The effective temperature: a change of ± 100 K corresponds to about ± 0.3 dex in the required Ti abundance.
6. The surface gravity: a change of ± 0.5 dex in log g corresponds to about ∓ 0.15 dex in the required Ti abundance.

Non-LTE effects are possible contributors to the apparently low Ti abundance. If the density of neutral Ti atoms is less than the LTE predicted value in the region of TiO line formation, the actual TiO density will be less than our calculated (LTE) density even if LTE is appropriate for the calculation of the density of TiO molecules from the actual (ground state) Ti and O densities and for the formation of the TiO lines. Overionization of Ti atoms is a possible non-LTE effect, but it is difficult to imagine that this effect can be a major contributor to "the TiO problem" and yet have escaped discovery in analysis of Ti I lines.

Inspection of these uncertainties shows that it is possible to account for the apparently low Ti abundance; for example, the correction for K_p and an upward adjustment to account for the lower gravity determined by Kovács (1983) (log g = 1.02) give log ϵ(Ti) = 4.55. If the effects of the uncertainties ΔD_0, Δf, and $\Delta[\epsilon(O) - \epsilon(C)]$ are combined quadratically, their total contribution is Δ log ϵ(Ti) = ± 0.2. Finally, an increase of $T_{\rm eff}$ by 100 K increases log ϵ(Ti) by 0.3 dex. This increase is partly offset by the need to raise the Ti abundance required to fit the Ti I lines. This shows that it may be possible to reconcile the TiO lines and the Ti abundance determined from Ti I lines.

When the TiO lines are strong, as in the cooler stars, a blanket of much weaker TiO lines provides a quasi-continuous opacity. It is certainly possible to fit α Tau's TiO lines with the expected near-solar Ti abundance by adding quasi-continuous opacity. However, this approach necessarily requires a high abundance [M/H] $\simeq +0.6$ to fit atomic lines near 7900 Å, an abundance in sharp disagreement with the metal abundances provided by atomic lines in regions uncontaminated by TiO lines.

For the coolest stars in the sample, addition of a quasi-continuous opacity is necessary in order to fit the TiO lines. In addition, a Ti abundance close to the abundance derived from Ti I lines (or inferred from Fe I and other lines in TiO-free regions) is needed in combination with the quasi-continuous opacity in order that the various atomic lines near the Rb I line give the expected [M/H]. For the cool S star TV Aur for which the predicted TiO intensities are sensitive to the adopted C/O ratio, we found it necessary to increase the ratio given by Smith & Lambert (1990) in order to fit the weak TiO lines but the increase was within the range permitted by the quoted uncertainties for the C and O abundances.

For representative stars, the Rb abundance was derived for several combinations of Ti abundance and quasi-continuous opacity κ(TiO). As noted earlier, the Rb abundance expressed as [Rb/M] is insensitive to the chosen combination as long as [M/H] is derived from the atomic lines around the Rb I line. As an illustration of this result, we shall cite results from three attempts at fitting the observed spectrum of HR 2508 ($T_{\rm eff}$ = 3600 K, log g = 0.7) which has a metal abundance [M/H] = +0.1 (Smith & Lambert 1990). This metallicity is provided by the metal lines near 7800 Å when the TiO lines are computed for a Ti abundance log ϵ(Ti) = 4.50 (i.e. [Ti/H] = −0.56) and the quasi-continuous opacity is set at κ(TiO) = 3.2 in arbitrary units. The Rb abundance corresponds to [Rb/M] = −0.4. Alternative fits with [Ti/H] = 0.1, κ(TiO) = 3.2 and [Ti/H] = −0.96, κ(TiO) = 0.0 give [Rb/M] = −0.3 and −0.5, respectively. The range in [Rb/M] of ± 0.1 is comparable to the uncertainty in matching the observed spectrum with a synthetic spectrum. These three fits correspond to a particular placement of the continuum. Tests show that [Rb/M] is similarly insensitive to the choice of a continuum level.

Comparisons of synthetic and observed spectra are shown in Figures 2 to 5. The spectrum of β And (Fig. 2) is representative of the M giants (and α Tau). The Rb I 7800 Å is clearly present but blended with the Si I line and several TiO and CN lines. A factor of 2 (0.3 dex) change of the Rb abundance produces a large change in the depth of the 7800 Å blended feature. The excellent fit of the synthetic to the observed spectrum of the intrinsic S star HD 64332 (Fig. 3) is typical of these s-process enriched warm stars. In this case, the Si I line is almost resolved from the Rb I line. The strongest Rb I line is seen for the cool intrinsic S star TV Aur (Fig. 4); a synthetic spectrum with a vanishingly small Rb abundance shows that Rb I provides the dominant contribution to the strong line near 7800 Å. The fit of the synthetic spectrum away from the Rb I blend is less satisfactory than for HD 64332. As a final example, we show observed and synthetic spectra for the extrinsic S star HD 35155 which has an unusually high neutron exposure, i.e., large

[5] We adopt the usual notation: $[X] \equiv \log_{10}(X)_{\rm star} - \log_{10}(X)_{\odot}$ for any abundance quantity X, and log $\epsilon(X) \equiv \log(N_X/N_{\rm H}) + 12.0$.

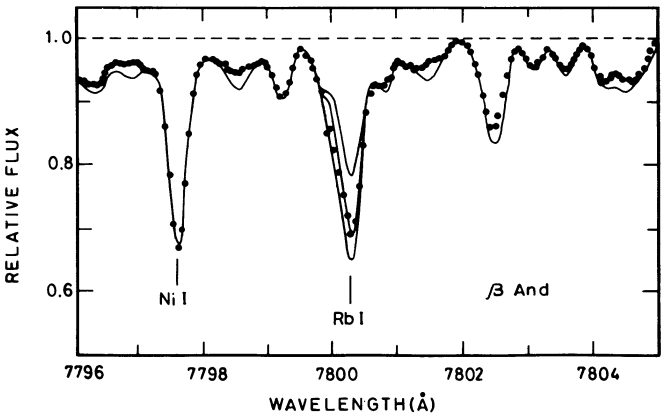

FIG. 2.—Observed (*filled circles*) and synthetic spectra (*thin lines*) of the M giant β And around the Rb I 7800 Å line. Synthetic spectra are shown for the Rb abundances [Rb/M] = −0.7, −0.4, and −0.1.

overabundances of Nd and other rare-earths but moderate overabundances of the lighter *s*-process elements such as Sr, Y, and Zr. Unidentified lines presumably attributable to rare earth atoms or ions are quite numerous around 7800 Å (and elsewhere) and two are labeled in Figure 5.

Our results are summarized in Table 1, where the stellar parameters ($T_{\rm eff}$, g), metallicity [M/H], and the *s*-process enhancement [*s*/M] are taken from Smith & Lambert (1990), where *s* here denotes Y and Zr. The fit of the synthetic spectra to the observed spectrum gives [Rb/M] which is computed from [Rb/H] and [M/H]. This [M/H] is not necessarily identical to the value given by Smith & Lambert (1990), but, as explained above, [Rb/M] is insensitive to how the TiO lines and quasi-continuous opacity are represented. In expressing the stellar Rb abundances as [Rb/M] on [Rb/H], we adopt the meteoritic Rb abundance given by Anders & Grevesse (1989): log ϵ(Rb) = 2.4 ± 0.03. The solar photospheric Rb abundance based on published (Hauge 1972) and unpublished (Grevesse 1984) analyses of the 7800 and 7947 Å Rb I lines is slightly higher: log ϵ(Rb = 2.60 with ±0.15 as an estimated uncertainty. If the photospheric Rb abundance is preferred as the reference point, the [Rb/M]-values in Table 1 will have to be

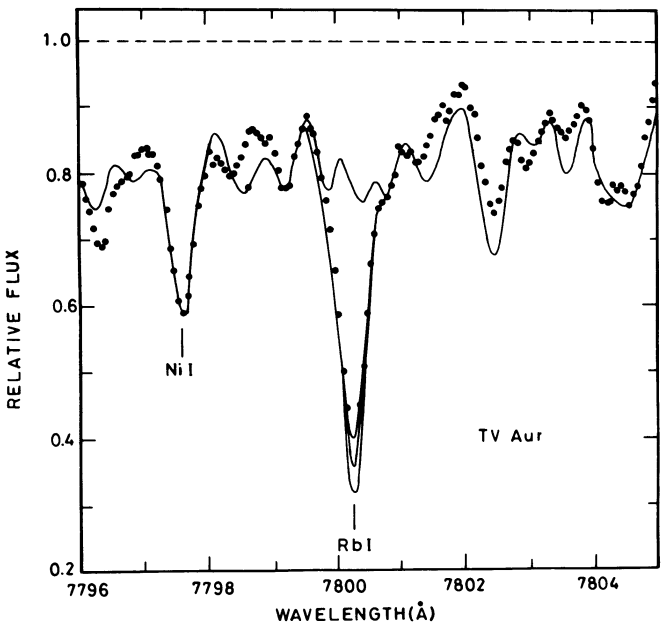

FIG. 4.—Observed (*filled circles*) and synthetic spectra (*thin lines*) of the cool intrinsic S star TV Aur around the Rb I 7800 Å line. Synthetic spectra are shown for [Rb/M] = +1.2, 0.9, 0.6, and −5 (no Rb).

decreased by 0.2. The presence or absence of Tc is noted in Table 1: intrinsic MS/S stars have Tc and the extrinsic (binary) MS/S stars do not have Tc.

3.3. *The s-process Rubidium in MS/S and Barium Stars*

In material of solar system composition, the *s*-process in the Kr-Rb region is resolvable into two components having different origins in terms of physical parameters and presumably of stellar sites (see Käppeler et al. 1989). The "weak" component, which is the dominant contributor to elements lighter than about Kr, is probably synthesized in the He-burning layers of massive stars. The "main" component, which is the dominant contributor to elements heavier than about Kr, is synthesized in the He shell of low-mass AGB stars and is the component whose effects are seen in the MS/S and barium stars. In addi-

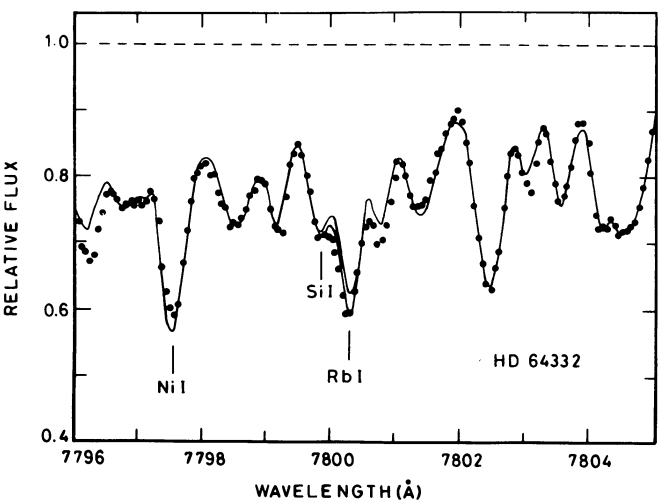

FIG. 3.—Observed (*filled circles*) and synthetic spectra (*thin lines*) of the intrinsic S star HD 64332 around the Rb I 7800 Å line. Synthetic spectra are shown for [Rb/M] = +0.2 and 0.0.

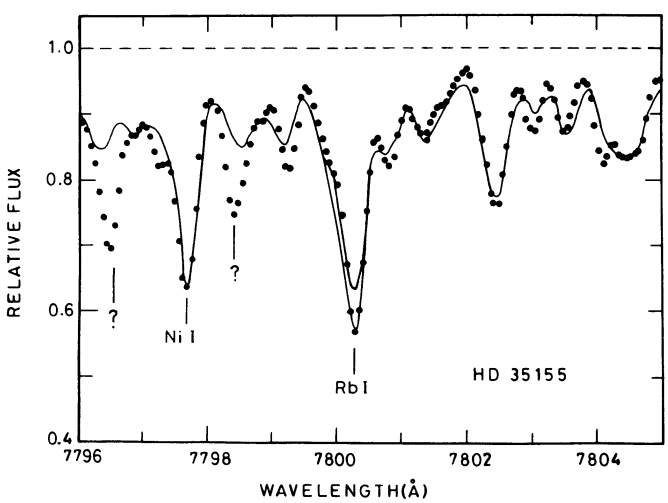

FIG. 5.—Observed (*filled circles*) and synthetic spectra (*thin lines*) of the extrinsic S star HD 35155 around the Rb I 7800 Å line. Synthetic spectra are shown for [Rb/M] = +0.1 and −0.2.

tion, the *r*-process contributes to the solar abundances, and this component is likely to be synthesized in supernovae of Type II (i.e., massive stars). A separation of the solar main component from the weak component and the *r*-process contributions is provided by Käppeler et al. (1989, their Table 4) for the neutron density $N(n) = 2 \times 10^8$ cm^{-3} and temperature $T = 2.7 \times 10^8$ K with the following results: $F = N(\text{main})/N(\text{total}) = 0.36$ for Rb, 0.69 for Sr, 0.61 for Y, and 0.68 for Zr. This separation is dependent on several factors including the adopted neutron density derived from analyses of several branches. (The Rb/Sr = 0.16 ratio for the solar main component is nearly a factor of 3 larger than the mean ratio reported for the barium giants.) The *r*-process is primarily responsible for the difference $N(\text{total}) - N(\text{main})$; $N(r)/N(\text{total}) = 0.6$ for Rb and 0.2 for Zr.

Since the principal effect of the neutron density on the ^{85}Kr branch is to change the abundance of Rb relative to the abundances of neighboring elements, we show in Figure 6 the abundance [Rb/M] versus [*s*/M], where [*s*/M] is the mean of [Y/M] and [Zr/M]. The values for [*s*/M] and [M/H] are taken from Smith & Lambert (1990). We also show results for five barium stars: HR 774 (Tomkin & Lambert 1983), ζ Cap (Smith & Lambert 1984), HD 121447 and HD 178717 (Malaney & Lambert 1988; Smith 1984), and *o* Vir (Tomkin & Lambert 1986). In each case, the barium star was analyzed relative to a normal giant of similar temperature and gravity; Tomkin & Lambert (1983) demonstrated that such a differential comparison serves to cancel almost completely the effects due to non-LTE. Our results for the M, MS, and S stars are similarly presented as abundances relative to α Tau. Since [M/H] and [*s*/M] are on average zero for the M giants, our abundances for the MS and S stars are effectively differential values with respect to the M giants. Inspection of Figure 6 shows that Rb and *s*-process enrichments are well correlated and that the S stars and barium define the same Rb-*s* relation. The lack of scatter in Figure 6 in excess of that due to measurement errors suggests that the *s*-process enrichments have been provided from sites of similar characteristics (i.e., neutron density and, hence, Rb/*s* ratio).

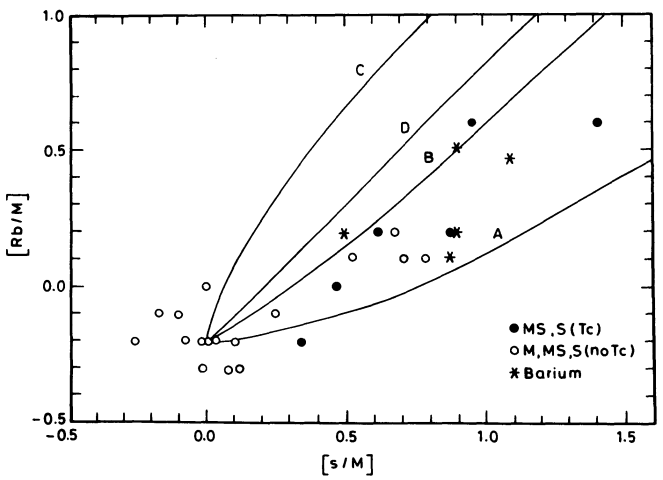

FIG. 6.—Observed and predicted correlations between rubidium and *s*-process enrichments for M, MS, and S stars and barium giants. Extrinsic and intrinsic MS and S stars are represented by open and filled circles, respectively. The predictions normalized to [Rb/M] = −0.2 and [*s*/M] = 0.0 (see text) correspond to enrichment with material of different Rb abundances: $a_{\text{Rb}} = \frac{1}{5}$, 1 and 5 for case *A*, *B*, and *C*, respectively. Case *D* shows the expected relation if the added material has the solar abundances of Rb and the *s*-process elements.

Enrichment of the envelope with *s*-processed material is modeled as the mixing of two layers: an *s*-process rich layer (here, identified as "pro" for processed) and an envelope. Since the processed material from the He-shell is expected to be very enriched in *s*-process elements, a small mass (M_{pro}) from the *s*-process rich layer may be added to the mass of the envelope (M_{env}) to achieve the observed *s*-process enrichments. Under this condition, the *s*-process enrichment is given by

$$\left[\frac{s}{\text{M}}\right] = \left(1 + \frac{Z_{\text{pro}}(s)}{Z_{\text{env}}(s)}\frac{M_{\text{pro}}}{M_{\text{env}}}\right),$$

where $Z_{\text{pro}}(s)$ and $Z_{\text{env}}(s)$ are the mass fractions of element *s* in the processed layer and the initial envelope respectively. Since the stars are generally of solar metallicity, we assume that the envelope's initial composition was solar: $Z_{\text{env}}(s) = Z_{\odot}^{\text{total}}(s)$, where the superscript "total" denotes that the element *s* may have *s*(main), *s*(weak), and *r*-process contributions. We neglect the very small contribution of the *p*-process. For $Z_{\text{pro}}(s)$, we write $Z_{\text{pro}}(s) = a_s Z_{\odot}^{\text{main}}(s)$ which reflects the idea that the main *s*-process component is synthesized in AGB stars and, hence, the stars in Figure 6 are likely to show enrichment by a main-like component rather than a weak-like component. Detailed analyses of barium and S stars confirm this supposition. With this expression for $Z_{\text{pro}}(s)$, the predicted enrichment becomes

$$\left[\frac{s}{\text{M}}\right] = \log\left(1 + a_s \frac{Z_{\odot}^{\text{main}}(s)}{Z_{\odot}^{\text{total}}(s)}\frac{M_{\text{pro}}}{M_{\text{env}}}\right).$$

Synthesis under similar conditions, but at different neutron densities, may be represented approximately by changing a_{Rb} but keeping a_s fixed for other elements. In Figure 6, we show predicted relations between [Rb/M] and [*s*/M] for $a_s = 1$ and different $a_{\text{Rb}} = \frac{1}{5}$, 1, and 5 (cases *A*, *B*, and *C*, respectively). We also show a prediction for $Z_{\text{pro}}(s) = Z_{\odot}^{\text{total}}(s)$ when, of course, [Rb/M] = [*s*/M]—see Case *D* in Figure 6. These predictions are matched to the observations at [Rb/M] = −0.2 and [*s*/M] = 0.0 which are the mean abundances given by our analyses of the normal M giants. Since observations of dwarf stars show that [*s*/M] $\simeq$ 0 for a sample of solar-metallicity stars (Edvardsson et al. 1993), our result that the M giants have [*s*/M] = 0 on average indicates the absence of systematic errors in the differential analysis. The Rb abundances in Table 1 are given relative to the meteoritic value. Our reference star α Tau has [Rb/M] = −0.2 (see also Plez et al. 1993). Since the normal M giants give a similar result, the Rb abundance of these stars expressed relative to α Tau is [Rb/M] $\simeq$ 0.0 on average. Observations (Woolf, Tomkin & Lambert 1995) of dwarf stars of near-solar metallicity show that the *r*-process abundances as measured by Eu increase slightly with decreasing metallicity, i.e., [*r*/M] > 0 for [M/H] < 0. We have not made the small correction for the variation in the ratio of main-*s* to *r*-process abundances because most of our stars have a roughly solar metallicity.

The fact that apparently all M giants and α Tau have a lower Rb abundance than the solar system deserves comment. (The warmer K giant β Gem has a solar Tb abundance.) There are several possible reasons for the apparent Rb deficiency of the M giants:

1. Rb has not been investigated in stars other than the *s*-process enriched stars referred to here and the few associated standard stars. In particular, dwarfs have not been examined for Rb. Therefore, we cannot at present exclude the Sun as being slightly Rb-rich relative to local stars of solar metallicity.

Moreover, nothing is known about the variation of Rb abundance with metallicity; we presume that [Rb/M] $\cong 0$ for normal stars of near-solar metallicity but possibly the Sun has an above-average Rb abundance.

2. The absolute Rb abundances of the M giants may be affected by a systematic error. One obvious possibility is that the ionization balance ($Rb \leftrightarrow Rb^+$) is not in LTE because the nonlocal ultraviolet radiation field ionizes the neutral atoms more completely than predicted for LTE. Use of α Tau as a standard star will certainly reduce the systematic error incurred by our use of LTE, as is suggested by the fact that [Rb/M] = 0 for M giants relative to α Tau. In addition an empirical cancellation of non-LTE effects was effected for the barium giants and significantly their Rb/M abundance ratios match well those of MS/S stars of the same *s*-process enrichment.

When the predictions are normalized as discussed, the Rb abundances of the MS and the S stars, as well as the barium stars, are best fitted by predictions corresponding to $a_{Rb} \simeq 0.3$ for $a_s = 1$. For the chosen normalization, the limits on a_{Rb} are approximately $a_{Rb} \simeq 1$ to 0.25, where $a_{Rb} = 1$ is a possible solution when alternative normalizations are chosen for the predictions (e.g., [Rb/M] = 0.4 and [*s*/M] = 0.0) but such alternatives do not really fit the compositions of the M stars. There is no convincing evidence for $a_{Rb} > 1$. Case C for $a_{Rb} = 5$ is representative of predictions for IMS models and is clearly excluded.

The ratio Rb/s for the *s*-processed material is related to the factors a_{Rb} and a_s. For example,

$$Z_{pro}(s) = a_s F(s) Z_{\odot}^{total}(s)$$

by definition and, hence,

$$\left(\frac{Rb}{Sr}\right)_{pro} \equiv \frac{Z_{pro}(Rb)}{Z_{pro}(Sr)} = \frac{a_s(Rb)}{a_s(Sr)} \frac{F(Rb)}{F(Sr)} \frac{Z_{\odot}^{total}(Rb)}{Z_{\odot}^{total}(Sr)} = 0.16 a_s(Rb)$$

which for $a_s(Rb) \simeq 0.3$ gives $(Rb/Sr)_{pro} \sim 0.05$ for the *s*-processed material.

Wallerstein (1992) derived a Rb abundance for the S star R And from an observation of the Rb I 7800 Å and K I 7699 Å resonance lines in emission. Simple assumptions about the excitation mechanism led to the abundance ratio [Rb/K] $\cong$ [Rb/M] $\simeq 1.0$. Analyses quoted by Wallerstein give [*s*/M] $\simeq +0.8$. With these abundances, R And falls above the results plotted in Figure 6, where relative to [Rb/M] $= -0.2$, [Rb/M] $\simeq +0.5$ for [*s*/M] $\simeq -0.8$. Unfortunately, the photospheric Rb abundance cannot be derived for R And. It should be noted, however, that Wallerstein's result is based on crude estimates for the excitation cross sections of these resonance lines and perhaps more importantly, mutilation of the emission lines by circumstellar absorption was ignored. The latter effect, which is surely present as Tsuji (1971) reports a circumstellar Rb I for R And, would be expected to affect the K I line more than the Rb I line. Then, [Rb/K] and hence [Rb/M] may have been overestimated.

4. THE ZIRCONIUM ISOTOPIC ABUNDANCES

4.1. *Basic Data for* ZrO

Two electronic systems of ZrO contribute lines across our bandpass. The primary target of our observations was the 0–1 band of the $B\,^1\Pi$–$X\,^1\Sigma^+$ system with its *R* branch bandhead at 6931.7 Å for ^{90}ZrO. Phillips & Davis (1976) give a line list for the 0–1 and other bands of the ^{90}ZrO molecule, and a set of molecular constants. We incorporated the latter into a computer program that reproduced the ^{90}ZrO lines' frequencies and predicts frequencies for the isotopically substituted molecules. This line list is a complete representation of the $B-X$ system's contribution to the observed bandpass. The *gf*-values for the lines are computed from the relation

$$gf_{line} = f_{v'v''} \frac{S_{J'J''}}{2} \frac{\sigma_{J'J''}}{\sigma_{v'v''}}, \quad (1)$$

where $f_{v'v''}$ is the band *f*-value, $S_{J'J''}$ is the rotational line strength or Hönl-London (HL) factor, $\sigma_{J'J''}$ and $\sigma_{v'v''}$ are the line and band frequencies, respectively. We adopt $f_{01} = 0.59 \pm 0.20$ (and $\sigma_{v'v''} = 14414$ cm^{-1}), the experimental value given by Littleton & Davis (1985) who performed a rotational line analysis of an emission spectrum and estimated the *f*-value relative to that of the β system ($c\,^3\Pi$–$a\,^3\Delta$) for which an absolute *f*-value was obtained from a measurement of the radiative lifetime of the $c\,^3\Pi$ state. The HL-factors are $S_{J'J''} = J'' - 1$, $2J'' + 1$, and $J'' + 2$ for the *P*, *Q*, and *R* branches, respectively. The defining relation for the *gf*-values assumes that the electronic transition moment (R_e^2) is independent of internuclear separation and that the band *f*-value is independent of rotational quantum number (i.e., the Franck Condon factor, $q_{v'v''}$, is independent of J' and J''). Failure of these assumptions is expected to have only a small effect of the *gf*-values and no effect at all on the isotopic analysis.

A blanket of lines from the $\Delta v = -1$ sequence of the γ-system ($A\,^3\Phi$–$X'\,^3\Delta$) contaminate the bandpass. The 1–2 band's R_1 branch, ^{90}ZrO bandhead, which is at 6923.4 Å, is a prominent feature of our spectra. Lines from the 0–1 to 9–10 bands are predicted to occur within our bandpass. Frequencies for these lines were predicted using the equations and molecular constants given by Phillips & Davis (1979). Comparison of predicted and observed (J. G. Phillips 1979, private communication) wavelengths for the 0–1 to 4–5 bands led to empirical corrections which were included in the final construction of the line list. Bands 5–6 to 9–10 have not been subjected to a rotational analysis and molecular constants for these high vibrational levels are unknown except by extrapolation. We chose arbitrarily to apply the wavelength correction derived for the 5–6 band to each of the higher members of the sequence. Their collective high line density and low predicted strength in the stellar spectra ensure that precise knowledge of the wavelengths of individual lines is not a major source of uncertainty in our isotopic analysis.

The *gf*-values for the γ-system lines are based on the absolute band *f*-value, $f_{00} = 0.57 \pm 0.17$ for $\sigma_{00} = 15741$ cm^{-1}, measured by Littleton & Davis (1985). On the assumption that $R_e^2(\gamma)$ is independent of internuclear separation, the *gf*-value for a line in our list is given by the expression

$$gf_{line} = f_{00} \left(\frac{q_{v'v''}}{q_{00}}\right) \frac{\sigma_{line}}{\sigma_{00}} S_{J'J''},$$

where the Franck-Condon factors are taken from Bell et al. (1979). For ease of computation, we obtain $S_{J'J''}$ from the expression from Hund's coupling case (*a*) (Tatum 1968). Comparison of the HL factors for case (*a*) and intermediate coupling show that the former are too large by about 2% at $J'' = 100$. In effect, this difference is distributed among several satellite branches which we omit from our line list. Our strict

separation of vibration and rotation is also source of a small error. Bell et al. (1979) predict how the Franck-Condon factor, $q_{v'J'v''J''}$, varies with rotational quantum number for the limiting case in which R_e^2 is independent of internuclear separation, e.g., for the Q branch of the 1–2 band, $q = 0.155$ at low J-values and increases to $q = 0.176$ at $J'' = 100$. The predicted increase decreases slightly along the sequence. Our gf-values are based on the "rotationless" $q_{v'v''}$ factors tabulated by Bell et al. (1979). Finally, the excitation potentials of the lower levels are computed taking account of the singlet-triplet separation of 1387 cm^{-1} (Hammer & Davis 1980). A dissociation energy $D_0 = 8.00 \pm 0.14$ eV (Pedley & Marshall 1983) was adopted for ZrO. In the final fitting of synthetic to observed spectra, a scaling factor, effectively the Zr abundance, is employed.

4.2. *Spectrum Synthesis and the* Zr *Isotopic Abundances*

For the Zr isotopes to be cleanly detected and then analyzed for the isotopic abundances, the ZrO features must be strong enough. The observed strong S stars are typically overabundant in the heavy s-process elements by a factor of 10–30. With such large s-process overabundances, many heavy-element atomic lines fall throughout this region. Two S stars with weak ZrO were useful as templates with which to map the heavy-element lines: HR 8714 and RZ Lep. HR 8714 is a hotter S star with very weak ZrO, while RZ Lep is a cooler S star, but with a C/O ratio of almost unity and, thus, very weak ZrO bands but extremely strong heavy-element lines. Using Kurucz & Peytremann's (1975) line list, these strong lines were identified with, mostly, very heavy element s-process lines. For weak ZrO bands and relatively strong heavy-element lines, the bandheads of the weaker Zr isotopes are severely blended and difficult, if not impossible, to analyze reliably. We analyze only those S stars in which the ZrO bands dominate the atomic absorption. This restricted us to the strongest S types and we discuss here R And, BI And, T Cam, S Cas, U Cas, AD Cyg, and R Gem. We presume that these are most probably intrinsic S stars; Little, Little-Marenin, & Bauer (1987) surveyed S stars for Tc and remark that single S stars show Tc I lines in their spectra. Tc is known to be present in R And, T Cam, U Cas, and R Gem. We are unaware of a search for Tc in BI And, S Cas (Li I is strong), and AD Cyg.

All of the observed S stars are cool variables for which we have very limited spectral information: we have no way of determining a well-defined $T_{\rm eff}$. Using the set of model atmospheres used for the Rb I analysis, we synthesized the ZrO bands for models with log $g = 0.0$ (the lowest in the grid) and $T_{\rm eff} = 3000$, 3200, and 3600 K. As the program stars were all strong S stars, we set the C/O ratio equal to 0.98 in all cases. We also used a microturbulent velocity of $\xi = 5$ km s^{-1} as we found that this best reproduced the relative depths of features both inside and outside of the ZrO bandheads. The hotter models ($T_{\rm eff} = 3400$ and 3600 K), with typical zirconium abundance enhancements of [Zr/H] = +0.8–1.0, yielded satisfactory fits to the ZrO bandheads. Lower $T_{\rm eff}$-values of 3000 and 3200 K resulted in synthetic ZrO bandhead depths, relative to the spectral intensities just outside of the bandheads, that were always too deep no matter the value of microturbulent velocity, C/O ratio, or [Zr/H]. This discrepancy could be alleviated by truncating the model atmospheres at optical depths of $\tau(1\ \mu m) = 5 \times 10^{-3}$, as opposed to $\tau(1\ \mu m) = 1 \times 10^{-5}$ for the hotter models. Either these S stars are hotter examples of these late-type stars, or the models are incomplete representations of the real stars at very low continuum optical depths. This is not surprising as it is known that these cool, variable S stars are losing mass, and the "top" of the atmosphere, τ(top), is not a well-defined quantity, thus the truncated optical depth of the model atmosphere is an arbitrary value. Using the S star R And with the strongest ZrO bands as a test, we find very little (if any measurable) effect of changing $T_{\rm eff}$ or τ(top) on the derived isotopic abundances of Zr.

In Table 2 we present estimated isotopic abundances of Zr for each star, band, and spectral resolution deemed useful. Since we have no reliable indicators of the star's $T_{\rm eff}$ the Zr-isotopic fractions listed in Table 2 were all derived for the model atmosphere with $T_{\rm eff} = 3200$ K, log $g = 0.0$, $\xi = 5.0$ km s^{-1}, and C/O = 0.98. Our main effort was to detect ^{96}ZrO and, in this analysis, it is clear that we cannot claim detection of the ^{96}ZrO bandhead, either for the γ 1–2 or $B-X$ 0–1 systems. A conservative estimate would place our upper limits at 5%, although in many syntheses, especially for the $B-X$ 0–1 system, even fractional abundances of 0.02 for ^{96}Zr are predicted to produce a measurable depression. In Figure 7, we show a sample spectrum plus syntheses for the star T Cam, illustrating the $B-X$ 0–1 band. Note the very low excitation (0.06 eV) Y I line. The Y I line either shows multiple components or a central emission peak. Note also the heavy-element lines Dy I and Ir I which bracket the expected ^{96}ZrO bandhead. A comparison of observed and synthetic spectra of the γ 1–2 bandheads for R And was given by Lambert (1988).

The shape of the ZrO absorption bands is remarkably similar from star to star. In all cases, the maximum absorption occurs clearly at the position of the ^{90}ZrO bandhead (in both the Π–Σ and γ-systems). Even in the case of strong atomic-line absorption, where the individual isotopic bands are obscured, the underlying ZrO absorption can be traced and the absorption is always "undetectable" at the ^{96}ZrO bandhead and is a maximum at the ^{90}ZrO bandhead. Quantitative estimates of our uncertainties in determining the isotopic abundances are not trivially obtained as several complex effects play a role:

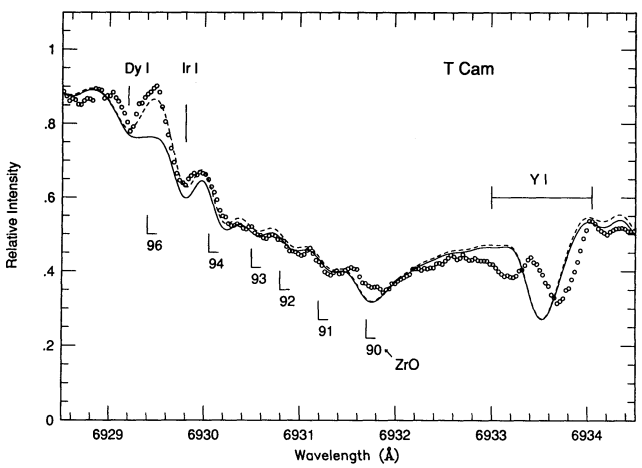

FIG. 7.—Observed (*filled circles*) and sample ZrO synthetic spectra for the S star T Cam. The $B-X$ 0–1 bandheads are synthesized for two difference isotropic mixtures of Zr: the solid line is a synthesis with no ^{96}ZrO in the mixture, while the dashed line contains a fractional content of 0.04 ^{96}Zr. The two atomic absorption lines near the ^{96}ZrO bandhead are noted (Dy I and Ir I) and illustrate the need for care in examining and synthesizing the S stars. Clearly, no absorption from ^{96}ZrO is indicated to a rather small fraction, i.e., $f \lesssim 0.02$. In addition, we note the complicated feature near in the observed spectrum near the expected position of a low-lying (0.05 eV) Y I line. In many of the S stars, this line changes shape and position and we suspect that circumstellar absorption and emission may contaminate this line.

model atmosphere effects, saturation of the bands, and the overlying presence of heavy-element atomic absorption lines probably represent the largest unknowns. From an observational point of view, spectra of the same star taken of the $B\ ^1\Pi$–$X\ ^1\Sigma^+$ transition in R Gem on two dates (see Fig. 1) yields the following isotopic fractions: 90–0.38 and 0.32, 91–0.17 and 0.23, 92–0.15 and 0.11, 93–0.05 and 0.02, 94–0.21 and 0.29, and upper limits of 0.04 on ^{96}Zr. As listed, differences of 0.05–0.08 in the fractional abundances are possible. A comparison of the $B\ ^1\Pi$–$X\ ^1\Sigma^+$ to the γ-system in the same star (on the same date) gives comparable differences of 0.04–0.08 (in T Cam, R And, and AD Cyg). Uncertainties of 5%–8% thus appear typical for the isotopic fractions, and probably represent an upper limit to how well the isotopic abundances can be determined. As noted above, the derived isotopic abundances are insensitive to the selected model atmosphere. We emphasize that in no S star can we claim a positive detection of ^{96}ZrO and, as this is the least saturated of any of the ZrO absorption features, a conservative upper limit in all of the stars is 5%.

Stars with weak ZrO or strong atomic lines were not subject to spectrum synthesis. These stars where ^{96}ZrO absorption is absent include: TV Aur, R Cam, WX Cam, AA Cyg, FF Cyg, R Cyg, V441 Cyg, T Gem, R Lyn, V812 Oph, SX Peg, GG Pup, T Sgr (*very* strong heavy-element lines and very Li rich!), S UMa, EP Vul, and BD +44°2267. Intrinsic rather than extrinsic (binary) S stars must dominate this list. Technetium, an indicator of an intrinsic S star, is known to be present in AA Cyg, R Cyg, T Gem, T Sgr, and S UMa (Little et al. 1987). A search for Tc I lines has yet to be made in spectra of the other stars.

Derived isotopic abundances are presented in Table 2. Two points are immediately obvious. Most important from the point of view of exploitation of ^{96}Zr as a neutron densitometer is our failure to detect this isotope in a single S star: a limit $^{96}\mathrm{Zr}/\mathrm{Zr} < 0.02$ is set in several cases and the upper limit $^{96}\mathrm{Zr}/\mathrm{Zr} < 0.05$ is a firm value for all stars. Since the S stars with ZrO bands are heavily enriched in *s*-process products, the observed atmospheric relative abundances of *s*-process products are effectively the relative abundances at the *s*-process site. Viewed another way, the original abundance ratio of ^{96}Zr/Zr in the atmosphere is diluted appreciably as *s*-process products free of ^{96}Zr are added. For example, $^{96}\mathrm{Zr}/\mathrm{Zr} \simeq 0.03$ for the solar system becomes $^{96}\mathrm{Zr}/\mathrm{Zr} \approx 0.003$ for a factor of 10 enrichment of the envelope, i.e., the star's original ^{96}Zr abundance is diluted appreciably and ^{96}Zr/Zr remains below our detection limit unless the *s*-process products contain ^{96}Zr.

The second point is that the isotopic abundances, as derived from echelle spectra, are remarkably similar from star to star. The scatter may be due entirely to the errors of measurement. An unweighted mean of the "echelle" results in Table 2 is $^{90}\mathrm{Zr}:^{91}\mathrm{Zr}:^{92}\mathrm{Zr}:^{93}\mathrm{Zr}:^{94}\mathrm{Zr}:^{96}\mathrm{Zr} = 0.35:0.16:0.16:0.07:0.22:<0.03$. Several stars for which grating but not echelle spectra were obtained do appear to have a somewhat different isotopic mix, i.e., higher ^{90}Zr abundance. Since grating and echelle spectra of R And yield similar isotopic abundances, we suppose that the different isotopic mixes from grating spectra are not entirely attributable to the lower resolution of the grating spectra. It is of interest to note that fits of synthetic spectra to the observed spectra are of a decidedly inferior quality when ^{93}ZrO's contribution is omitted. This unstable but long-lived ^{93}Zr isotope is present in these atmospheres because it is on the main *s*-process path.

Our results are compatible with the few published results based on inferior spectra and a simpler construction of synthetic spectra. Zook's (1985) analysis of the $B-X$ 0–1 bandhead in R Cyg and V Cnc gave mean ratios $^{90}\mathrm{Zr}:^{91}\mathrm{Zr}:^{92}\mathrm{Zr}:^{93}\mathrm{Zr}:^{94}\mathrm{Zr}:^{96}\mathrm{Zr} = 0.47:0.10:0.17:0.06:0.20:0.00$ which apart from a minor change in the $^{90}\mathrm{Zr}/^{91}\mathrm{Zr}$ ratio closely resemble our results. Peery & Beebe (1970) found an even higher $^{90}\mathrm{Zr}/^{91}\mathrm{Zr}$ (= 10) ratio for R Cyg from analysis of the γ-system's 0–0 band for which the self-blending for ZrO lines is severe.

On the generally held supposition that S stars are representative of the stars that contribute *s*-processed material to the interstellar medium, we expect a close correspondence between the isotopic Zr abundances of the S stars and the solar system. A direct comparison is frustrated by the fact that the *r*-process and the weak *s*-process as well as the main *s*-process have contributed to the solar system abundances. According to Käppeler et al. (1989) the weak *s*-process contribution is about 10% that of the main component. The *r*-process contribution has essentially to be found by modelling the *s*-process contribution using *s*-only nuclei of higher and lower atomic number. Toukan & Käppeler (1990) using neutron capture cross sections similar to those recommended by Beer et al. (1991) report such an allocation of the solar system abundances into *s*- and *r*-process contributions for the even Zr isotopes, i.e., $^{90}\mathrm{Zr}:^{92}\mathrm{Zr}:^{94}\mathrm{Zr} = 40 \pm 3:12 \pm 2:19 \pm 1$ which compares favorably with the mean results of 38:16:21 from Table 2. The ratio $^{91}\mathrm{Zr}:^{92}\mathrm{Zr} = 12:14$ for the solar *s*-process contribution according to Käppeler et al. (1989) is quite similar to the mean stellar ratio of 11:17 considering the uncertainties in these ratios. The solar system's ^{96}Zr is reasonably attributed almost entirely to the *r*-process and the *s*-process contribution ($^{96}\mathrm{Zr}/^{94}\mathrm{Zr} = 0.07 \pm 0.05$ according to Toukan & Käppeler 1990) is consistent with our failure to detect the ^{96}ZrO bandheads ($^{96}\mathrm{Zr}/^{94}\mathrm{Zr} < 0.14$). It is also interesting to note that the solar system's inferred *s*-process abundance of ^{93}Nb, the nuclide formed from the decay of ^{93}Zr, is about 6% of the total Zr abundance and in agreement with the mean stellar ^{93}Zr abundance of 7%.

5. THE NEUTRON DENSITY

In this section, we discuss the constraints imposed on models of AGB stars by our observations of Rb and Zr in MS and S stars. Our analyses of the Rb I line as well as previous work on barium giants shows that the *s*-processed material has an abundance ratio Rb/Sr $\approx$ 0.05. The ZrO analyses show no evidence of ^{96}Zr at a level $^{96}\mathrm{Zr}/\mathrm{Zr} \lesssim 5\%$. After discussion of the ^{85}Kr and ^{95}Zr branches that control synthesis of Rb and ^{96}Zr respectively, we consider published models of intermediate and low-mass AGB stars and conclude that only the latter can account for the reported abundances of the neutron-density sensitive Rb and ^{96}Zr.

5.1. *Predictions*

5.1.1. *Operation of the* ^{85}Kr *Branch*

Unstable ^{85}Kr provides a branch point in the *s*-process path that controls the rubidium isotopic abundances during operation of the *s*-process. Figure 8 from Beer & Macklin (1989) shows the principal segments of the *s*-process path at and beyond ^{85}Kr. The sensitivity of the Rb abundance to neutron density is readily illustrated. A critical density $N(n)_c$ may be defined such that the probability that the ^{85}Kr ground state will β-decay is equal to the probability that it will capture a

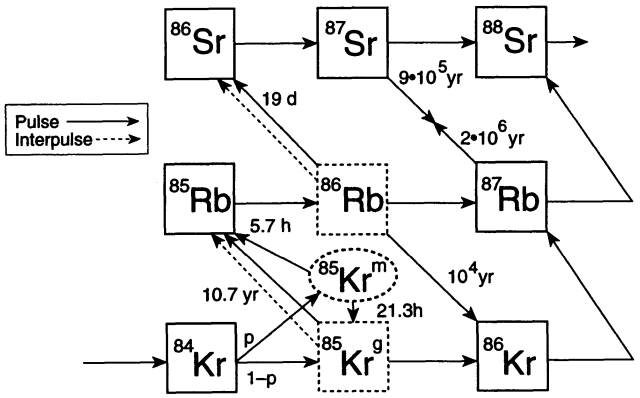

FIG. 8.—Synthesis of Kr, Rb, and Sr isotopes during a thermal pulse (*solid line*) and in the interpulse phase (*dashed lines*) when the ^{85}Kr and ^{86}Rb which are built up decay. The population p of the isomeric state of ^{85}Kr is generated by neutron capture on ^{84}Kr ($p = 0.52 \pm 0.006$; Beer et al. 1991). Half lives of unstable nuclei are indicated and, when temperature dependent, a temperature of 30 keV has been adopted. The time scales for ^{87}Rb and ^{87}Sr β-decay during the pulse are too long to be of any significance for the synthesis. The branching of ^{86}Rb to ^{96}Kr can be neglected too. The unstable nuclei ^{85}Kr and ^{86}Rb are represented by "broken" boxes; ^{87}Rb is effectively stable after manufacture. (After Beer & Macklin 1989.)

neutron to form ^{86}Kr. Let us adopt the following parameters: (1) a β-decay half life of 10.7 yr (we disregard for the moment ^{85}Kr's short-lived isomeric state); (2) a neutron capture cross section of $\sigma(^{85}\mathrm{Kr}) \simeq 67$ mb at 30 keV (Beer & Macklin 1989). Then, we find $N(n)_c \simeq 1.1 \times 10^8$ cm^{-3}. At a neutron density $N(n) \lesssim 10^7$ cm^{-3}, the s-process path runs essentially unbranched from ^{84}Kr to ^{85}Rb to ^{86}Sr via the unstable nuclei ^{85}Kr and ^{86}Rb; the critical density for the ^{86}Rb branch is $N(n)_c \simeq 3 \times 10^9$ cm^{-3}. At $N(n) \gtrsim 10^9$ cm^{-3}, a major part of the flow is from ^{84}Kr to ^{86}Kr, ^{87}Rb, and ^{88}Sr with a second minor branch proceeding as before to ^{85}Rb and ^{86}Sr. When the neutron density exceeds the critical density also for the ^{86}Rb branch, say $N(n) \gtrsim 3 \times 10^{10}$ cm^{-3}, the path from ^{86}Rb proceeds to ^{87}Rb and ^{88}Sr and the channel to ^{86}Sr is largely suppressed.

When a steady state flow along the path is attained, the density of a nuclide unaffected by a branch is given approximately by $\sigma_i N_i \simeq$ constant, where σ_i is the neutron capture cross-section of nuclide i. When the Rb isotopes are referenced to a nuclide k just before or after the branch, and the neutron density is either much less or much higher than the critical density (i.e., the flow is effectively unbranched), we expect

$$\sigma(^j\mathrm{Rb})N(^j\mathrm{Rb}) \simeq \sigma_k N_k \simeq \text{constant} ,$$

$$N(^j\mathrm{Rb}) \approx \frac{\text{constant}}{\sigma(^j\mathrm{Rb})} ,$$

where j denotes either ^{85}Rb at low neutron density or ^{87}Rb at high neutron density.

The sensitivity of the Rb elemental abundance to the neutron density arises then because the stable isotopes that dominate the abundance in the low (i.e., ^{85}Rb) and the high (i.e., the neutron magic ^{87}Rb) neutron density limits have quite different neutron capture cross sections: $\sigma(^{85}\mathrm{Rb}) = 240 \pm 9$ mbarn and $\sigma(^{87}\mathrm{Rb}) = 18 \pm 0.5$ mbarn at $kT = 30$ keV (Raiteri et al. 1993). Although the above scaling $N_i \propto 1/\sigma_i$ does not hold exactly for neutron magic nuclei, a strong sensitivity to the cross section remains such that we expect the elemental Rb abundance to increase by an order of magnitude from low to high neutron density. A complete analysis requires also consideration of the adjacent strong bottleneck in the s-process path at the neutron magic nucleus ^{86}Kr with its small neutron capture cross section: $\sigma(^{86}\mathrm{Kr}) = 3.3 \pm 0.2$ mbarn at $kT = 30$ keV (Beer, Voss, & Winters 1992). This bottleneck leads to an accumulation of this nucleus in the high neutron density limit. Although simplified these prelusive remarks show that the Rb abundance is a monitor of $N(n)$ at the s-process site.[6]

In real operation, two factors not considered in the above sketch affect the Rb abundance. The first complication is that neutron capture on ^{84}Kr leads not only to the long-lived ($\tau_{1/2} = 10.7$ yr) ground state of ^{85}Kr, but also to a short-lived ($\tau_{1/2} = 5.7$ hr) isomeric state: the branching ratio p (see Fig. 8) is experimentally determined to be $p = 0.52 \pm 0.06$ at 25 keV (Beer et al. 1991). Under the conditions prevailing in the He shell, the isomeric state is not expected to come into thermal equilibrium with the ground state (Ward 1977; Ward, Newman, & Clayton 1976; Ward & Newman 1978) so that in accurate modeling of the s-process during a thermal pulse, the isomeric state must be considered as effectively a distinct nucleus. Two modes of decay are possible for the isomeric state: a β-decay to ^{85}Rb with a probability of 80% and internal γ-transition to the ^{85}Kr ground state with a probability of 20%. Hence, the isomeric state provides a route to ^{85}Rb that remains open at neutron densities characterizing the s-process. The second complication is that the final products are dependent on the temporal variation of the neutron density. This variation is particularly pronounced in realistic stellar conditions such as the bursts of neutrons released in the He-shell during a thermal pulse. For example, a high Rb abundance (i.e., ^{87}Rb primarily) may be achieved at the peak of the neutron burst, but lower Rb abundances may be restored in the declining phase (the "freeze out") of a burst. These latter abundances will depend on the way the neutron density declines. In addition, the duration (Δt_n) of the neutron burst plays a role in determining the final Rb abundance. If Δt_n is shorter than the effective halflife of ^{85}Kr (i.e., the reciprocal of the total destruction rate given by the sum of the β-decay and neutron capture rates), little fresh ^{86}Kr and ^{87}Rb will be synthesized. At the end of the burst, the unstable ^{85}Kr decays completely before the onset of the next burst. In this way, short neutron bursts of high neutron density will synthesize less ^{87}Rb than is achieved in a steady flow at the same neutron density. (The final products are also sensitive to the temperature at the s-process site. In addition to the obvious dependence of the neutron capture rate on temperature, certain β-decay and electron capture rates are temperature dependent over the relevant interval of $T \lesssim 3 \times 10^8$ K—see Takahashi & Yokoi (1987) for ^{86}Rb, ^{87}Rb, and ^{87}Sr but the decay of ^{85} Kr is effectively constant for $T \lesssim 3 \times 10^8$ K. Electron capture rates are also dependent on the local mass density and composition.)

[6] The order of magnitude increase of the Rb abundance occurs as the isotopic composition changes from almost pure ^{85}Rb at low $N(n)$ to ^{87}Rb at high $N(n)$. Unfortunately the isotopic wavelength shifts are small and accompanied by hyperfine structure such that even in the absence of the TiO blanketing a measurement of the Rb isotopic ratio is almost impossible—see the discussion by Lambert & Luck (1976) of Rb in the K giant Arcturus. The Rb isotopic ratio can certainly not be measured for our MS/S stars. The Kr (through the isotope ^{86}Kr) and Sr isotopic ratios are also affected by the ^{85}Kr branch but neither ratio is measurable by spectroscopic means for MS/S stars.

Operation of the *s*-process around the ^{85}Kr branch has been studied in detail for He-shell flashes in both low-mass (LMS) and intermediate-mass (IMS) AGB stars. This classification of AGB stars denotes a change in the principal neutron source from ^{22}Ne(α, n)^{25}Mg in the 4–8 $M_\odot$ (intermediate-mass) models to ^{13}C(α, n)^{16}O in the low mass ($m \lesssim 4\ M_\odot$) models.

5.1.2. *Operation of the ^{95}Zr Branch*

Unstable ^{95}Zr with a half-life of 65 days provides a simple branch in the *s*-process path (Fig. 9) controlling the production of the stable isotope ^{96}Zr. Since the neutron capture cross section of this isotope is the smallest of the sequence $^{90-96}$Zr, ^{96}Zr may be the most common Zr isotope produced at densities in excess of the critical density for the ^{95}Zr branch: Toukan & Käppeler (1990) show the abundance ratio ^{96}Zr/^{94}Zr increasing from about 0.01 at $N(n) = 10^8$ cm^{-3} to about 0.2 at $N(n) = 10^9$ cm^{-3} and to 0.5 at $N(n) = 3 \times 10^9$ cm^{-3}. The critical density of the ^{95}Zr branch is about an order of magnitude higher than that of the ^{85}Kr branch controlling Rb synthesis. The principal reason for this is that the half-life of ^{95}Zr is more than an order of magnitude longer than that of the ^{85}Kr ground state; the neutron capture cross sections of the two nuclei are similar and the effect of the short-lived isomeric state of ^{85}Kr is to weaken the full impact of the ^{85}Kr branch. Other branches in the *s*-process path influence the synthesis of the two lightest Zr isotopes. At the neutron densities that result in synthesis of ^{96}Zr, the branch at ^{89}Sr will direct the major flow to unstable ^{90}Sr and, thence, to ^{91}Zr; little ^{89}Y and ^{90}Zr will be synthesized. The critical density of the ^{89}Sr branch is approximately 1.5 times that of the ^{95}Zr branch.

In summary, *s*-processing at low neutron densities [$N(n)$ less than a few times 10^8 cm^{-3}] produces the isotopes ^{90}Zr, ^{91}Zr, ^{92}Zr, ^{93}Zr, and ^{94}Zr such that the isotopic abundances are roughly set by $\sigma(^i\mathrm{Zr})N(^i\mathrm{Zr}) \simeq$ constant. Cross sections at 30 keV from the Beer et al. (1991) compilation are 21, 60, 33, 95, and 26 mbarn with approximately a 10% accuracy for the sequence ^{90}Zr ro ^{94}Zr. At higher neutron densities ^{96}Zr is produced. The neutron capture cross section for ^{96}Zr is $\sigma = 10.7 \pm 0.5$ mbarn at 30 keV (Toukan & Käppeler 1990). Predictions of the synthesized abundances of ^{96}Zr near the critical neutron density are sensitive to the neutron capture cross section of ^{95}Zr: Toukan and Käppeler consider σ to fall in the range 50–72 mbarn at 30 keV.

The isotope ^{93}Zr has such a long half-life (1.5 Myr at room temperature and little reduced at stellar temperatures) that it

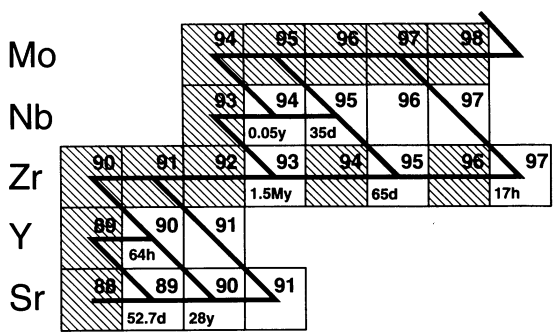

FIG. 9.—*s*-process path from Sr to Mo for neutron densities of 10^{10} cm^{-3} or less. Stable nuclei are represented by a striped box and unstable nuclei an open box in which the half life may be given—the half life of ^{94}Nb is quite temperature sensitive and the value for $T = 2 \times 10^8$ K is given. Major branches are given for neutron densities $N(n) \lesssim 10^{10}$ cm^{-3}.

may be considered a stable isotope when discussing the isotopic mix of Zr in intrinsic MS/S stars, (i.e., the thermally pulsing AGB stars). Extrinsic MS/S stars, however, would not be expected to show ^{93}Zr; note these are stars without Tc and the Tc isotopes have shorter half-lives than ^{93}Zr. With ^{93}Zr effectively a stable nuclide, the *s*-process path bypasses ^{93}Nb which is only synthesized from the decay of ^{93}Zr after *s*-processing has ceased (Busso et al. 1992).

5.2. *Intermediate-Mass AGB Stars*

For intermediate-mass AGB stars in which neutrons are supplied by the ^{22}Ne(α, n)^{25}Mg reaction, Malaney (1987) used published recipes for the neutron bursts and a thorough reaction network to predict the abundances of Rb and other elements. According to those recipes, the neutron bursts are characterized by a high peak neutron density, a duration of 1 month to a few years, and a rapid freezeout. The peak neutron density runs from $N(n)_{\rm pk} = 5 \times 10^9$ cm^{-3} for a C-O core mass (M_C) of 0.96 $M_\odot$ to about 2×10^{12} cm^{-3} for a C-O core of nearly the Chandrasekhar limit. Malaney predicted the Rb/Sr ratio in the He shell to reach the following values after many shell flashes: Rb/Sr $\simeq$ 1.0 at $M_C = 1.36\ M_\odot$, 0.7 at $M_C = 1.16\ M_\odot$, and 0.45 at $M_C = 0.96\ M_\odot$. Beer & Macklin (1989) describe similar calculations for core masses from $M_C = 0.65\ M_\odot$ to $1.16\ M_\odot$; these bursts at a given M_C are of slightly longer duration than Malaney's. The predicted Rb/Sr ratios decline from Rb/Sr $\simeq 0.6$ for $M_C = 1.16\ M_\odot$ [$N(n)_{\rm pk} \simeq 2 \times 10^{11}$ cm^{-3}] to 0.2 for $M_C = 0.65\ M_\odot$ [$N(n)_{\rm pk} \approx 3 \times 10^9$ cm^{-3}]. Busso et al. (1988) who also studied *s*-processing in IMS models investigated the sensitivity of the results to several quantities such as chemical composition and the neutron capture cross section of ^{22}Ne. For the value of the latter quantity corresponding to the precise experimental result of $\sigma(^{22}\mathrm{Ne}) = 0.06 \pm 0.005$ mbarn^{-1} (Beer et al. 1991; see also Nagai et al. 1991), Busso et al. (1988; see Busso et al. 1995) predict Rb/Sr $\simeq$ 1.5 to 4 for core masses in excess of 1.0 $M_\odot$. These calculations for intermediate-mass stars show that the *s*-process path at ^{85}Kr takes primarily the branch through ^{87}Rb and leads to a "high" Rb abundance and a nonsolar isotopic ratio.

Predictions of the isotopic Zr abundances were provided by Malaney (1986) for the suite of models mentioned above and by Busso et al. (1988). Malaney's adopted neutron capture cross sections differ by up to about 30% from currently recommended values (Beer, Voss, & Winters 1992) but we quote Malaney's results as published. The likely magnitude of the correction does not negate our conclusion that IMS AGB stars with massive cores predict ^{96}Zr in excess of our observed limits: for example, stars with $M_C = 1.16$ and $1.36\ M_\odot$ are predicted to have 18% and 22% of Zr in the form of ^{96}Zr and roughly equal abundances of ^{90}Zr, ^{91}Zr, ^{92}Zr, and ^{96}Zr. These predictions are clearly at odds with our observations (Table 2). The model corresponding to $M_C = 0.96\ M_\odot$ with peak $N(n) = 5 \times 10^9$ cm^{-3} predicts just 3% of the Zr to be ^{96}Zr and an isotopic mix that is roughly compatible with our observations. The Busso et al. (1988) calculations give ^{96}Zr to be 11%, a prediction that is too high to fit the observed stars.

The various predictions concerning the operation of the ^{85}Kr branch in IM AGB stars fail to match either the solar system relative abundances of Rb and Sr or the *s*-processed abundance ratios obtained from the MS/S and classical barium stars for which Rb/Sr $\simeq$ 0.05. This failure is one of several failures (see review by Lambert 1991) which has led to

pursuit of models of LMS (Malaney & Lambert 1988). Since the critical density of the ^{95}Zr branch is appreciably higher than that of the ^{85}Kr branch, the absence from S stars of ^{96}Zr serves to exclude only those IM AGB stars with the larger core masses as representating the S stars.

As an interim remedy for the failure of the IMS models, Beer & Macklin (1989) devised profiles for the neutron burst having the same basic shape as the IMS bursts but of lower neutron density. Exponential distributions of neutron exposures with neutron density profiles with peak densities of $N(n) \approx 10^8$–10^9 cm^{-3} gave Rb/Sr ≈ 0.07, which is representative of the values inferred from stellar observations. (In single exposure calculations, the Rb/Sr abundance ratios of the barium stars are reproduced only with still lower neutron densities: $N(n) \approx 10^7$–10^8 cm^{-3} [see Malaney & Lambert 1988]. Higher neutron densities such as those considered by Beer & Macklin are acceptable provided that the neutrons are supplied in bursts of short duration.) Although isotopic Zr abundances were not predicted it is clear that these models are consistent with the absence of ^{96}Zr from S stars.

The Beer & Macklin (1989) modified profiles for the neutron bursts do not, however, now appear to be a promising scenario for IMS models. New models including the effects of mass loss and of hydrogen burning at the base of the convective envelope (the so called phase of hot bottom burning) tend to reduce the maximum temperature attained in thermal pulses; Blöcker & Schönberner (1995) predict the asymptotic limit to be $T \simeq 3 \times 10^8$ K. A concomitant of the reduction of the maximum temperature is a sharp drop in the efficiency of the ^{22}Ne neutron despite the fact that recent measurements of the rate constant for ^{22}Ne(α, n)^{25}Mg reaction at the relevant temperatures show a factor of 3 or so increase over earlier adopted values (Käppeler et al. 1994). Although lower temperatures in the He shell imply a lower neutron density during the thermal pulses, the neutron exposure τ_0 is also reduced, as was found by Busso et al. (1988). Inspection of their computations for $T = 3 \times 10^8$ K and the "old" ^{22}Ne(α, n)^{25}Mg rate [a fair simulation of the case for the lower temperatures now preferred and the new ^{22}Ne(α, n)^{25}Mg rate] show a high Rb/Sr ratio ($\gtrsim 1.5$) due to the fact that the lower τ_0 affects Sr (particularly the neutron magic ^{88}Sr) more than Rb. There is apparently no way out: IMS models cannot provide the low Rb/Sr ratio observed in the barium giants.

5.3. *Low-Mass AGB Stars*

5.3.1. *The s-process in Thermal Pulses*

Since the predicted peak neutron densities decrease with decreasing C-O core mass, one might suppose that the Beer and Macklin (1989) empirical (extrapolated) profiles of neutron bursts might be identified with low-mass AGB stars. However, the extrapolations are invalid because the temperature in the He-burning shell decreases with decreasing core mass such that ^{22}Ne(α, n)^{25}Mg is only marginally operating or is even inactive in LMS. At the lower temperatures achieved in low mass AGB stars, the only efficient neutron source is the ^{13}C(α, n)^{16}O reaction provided that a sufficient amount of ^{13}C is synthesized at the H/He interface. Questions remain concerning the synthesis of adequate amounts of ^{13}C to run the *s*-process, especially for the neutron exposures observed in the Population I AGB stars (Iben 1991; Sackmann & Boothroyd 1991).

In models developed from a scenario originally devised for Population II AGB stars by Iben & Renzini (1982a, b), and Hollowell & Iben (1988, 1989), the thermal pulse in the He-burning shell leads to a double burst of neutrons. Gallino (1989) and Käppeler et al. (1990) discuss operation of the *s*-process in these circumstances. In the first burst, neutrons are generated from the ^{13}C(α, n)^{16}O reaction and, in the second and weaker burst, the neutrons are provided by ^{22}Ne(α, n)^{25}Mg, implying a consumption of ^{22}Ne by about 1% (Becker 1981). In the particular model examined by Käppeler et al. (1990), the ^{13}C burst has a peak neutron density, $N(n) \simeq 2 \times 10^9$ cm^{-3} for about 10 yr and a rapid freezeout that drops the neutron density by about a factor of 10 in 1 yr. In the second burst, which occurs about 20 yr later, the neutron density increases sharply to a peak value $N(n) \approx 10^9$ cm^{-3} and declines at once about as sharply such that $N(n)$ exceeds 10^8 cm^{-3} for less than 1 yr. In this model, the Rb abundance is set by the first burst and, relative to the majority of *s*-only nuclides, the Rb abundance exceeds the solar value by a factor of about 1.5. This excess reflects the peak neutron density in the first neutron burst. For these models of low-mass stars, the ^{13}C abundance in the He shell prior to ignition of the ^{13}C(α, n) reaction is not well constrained and was considered as an adjustable parameter.

Similar exploratory calculations were pursued by Busso et al. (1992), who also modeled the mixing of *s*-processed material to the surface during the so-called third dredge-up, i.e., the repeated penetration by the base of the outer convective envelope into the top of the He shell after each pulse. Predicted rubidium abundances of the convective H-rich envelope and atmosphere are given by Busso et al. (1995) who describe additional improvements to the calculations. Key assumptions influencing the neutron density of the *s*-process are the mass of ^{13}C synthesized from protons diffusing into the shell in the time interval between He-shell flashes and the rate of destruction of ^{13}C as the He shell flash develops. Busso et al. assume the mass of ^{13}C to be of the order of 10^{-6} $M_\odot$. This series of LMS models predicts the Rb/Sr ratio of the stellar atmosphere to be 0.15 which is up to about a factor of 2 less than the solar Rb/Sr ratio but above the upper end of the range found for our stars.

The level of agreement appears to be the best that one can expect from these models. The challenge is to find a way to reduce the neutron density without affecting too greatly the mean neutron exposure which is well constrained by the observed ratio of the abundances of heavy and light *s*-nuclides. The mean neutron exposure is set primarily by the mass of ^{13}C synthesized at the top of the He shell during the interpulse period as protons from the H-rich envelope are mixed into the top of the He shell and react there with ^{12}C nuclei. The neutron density prevailing in the thermal pulse is determined by the rate at which the ^{13}C is ingested into the thermal pulse. One might suppose that if the synthesized ^{13}C were to be distributed over a greater thickness at the top of the He shell, the rate of mass ingestion into the thermal pulse which is fixed for a given stellar model will necessarily result in a lower rate of ^{13}C ingestion and, hence, in a lower overall neutron density. This supposition is correct but there are quite severe constraints on the achievable reductions in neutron density. First, the thickness of the ^{13}C-enriched zone is unlikely to extend by more than one pressure scale height below the base of the H-rich envelope (Hollowell & Iben 1988). The mixing mechanism (diffusion or semi-convection) must necessarily be of low efficiency in order to be successful and, hence, the mass of the He shell contaminated with ^{13}C is small. (If the mixing mecha-

nism were efficient, ^{14}N not ^{13}C is the major product as ^{13}C is converted to ^{14}N by capture of another proton.) Second, even if the ^{13}C mass were widely distributed over the top of the He shell, a greatly lower neutron density is not necessarily achieved because much of the ^{13}C is then ingested into the thermal pulse early in its development when the temperature is below 1.5×10^8 K and the $^{13}C(\alpha, n)^{16}O$ rate is faster than the 3α process. Then, Bazan & Lattanzio (1993) found that energy generated from the $^{13}C(\alpha, n)^{16}O$ reaction modified the thermal pulse such that there was a sudden increase of the mass in the convective zones and a virtually instantaneous ingestion of the remaining ^{13}C and, therefore, a sharp *increase* of the neutron density, instead of the decrease that was sought. Our tests involving the thickness of the zone enriched in ^{13}C (and other tests) suggest that Rb/Sr $\simeq 0.15$ is a minimum ratio from the burning of ^{13}C during a thermal (convective) pulse. This minimum value exceeds that found for the Barium and MS/S giants by about a factor of 3.

Not unexpectedly, models of the low-mass AGB stars account quite satisfactorily for the absence of ^{96}Zr and the overall pattern of the isotopic Zr abundances. For example, the Busso et al. (1995) models predict $^{90}Zr:^{91}Zr:^{92}Zr:^{93}Zr:^{94}Zr:^{96}Zr \simeq 42:11:17:6:23:1.5$ for a variety of initial compositions and mean neutron exposures. These fractions compare favorably with the mean values from Table 2, where $^{90}Zr:^{91}Zr:^{92}Zr:^{93}Zr:^{94}Zr:^{96}Zr = 38:15:16:7:21:<3$.

5.3.2. *s-processing in the Interpulse Periods*

Straniero et al. (1995a, b) have analyzed in detail the fate of any ^{13}C produced below the H-rich envelope in LMS, following the evolving temperature conditions from the moment of the (assumed) production of ^{13}C through the interpulse phase and then through the next thermal pulse. They did so on the basis of their new stellar models that account self-consistently for dredge-up above a core mass of 0.65 $M_\odot$ for a star of initially 3 $M_\odot$ and solar composition. This value of the core mass was reached at the 14th pulse. In line with the ideas described in the previous section, they assumed that a certain amount of ^{13}C and ^{14}N (some 10^{-6} $M_\odot$) could be formed at the envelope/intershell border due to proton penetration during dredge-up. They found the intershell zone of their 3 $M_\odot$ model to experience an increasing temperature after dredge-up, so that the layers containing ^{13}C reached $T \simeq 1 \times 10^8$ K before the onset of the next pulse.

In the above environment, α-captures destroy ^{13}C on a timescale of some thousands years *before* the He shell ignites and becomes convective. The timescale for ^{13}C destruction is considerably longer than the episodes of neutron capture in a thermal pulse (convective He shell) so far referred to when discussing the pulsed *s*-process. Consequently, the neutron density associated with the low-efficiency (α, n) captures on ^{13}C is very low, never exceeding 2×10^7 cm^{-3}. This reduction of the neutron density (by a factor of at least 10 with respect to the lowest limit ever reached in convective pulses) is the sole essential change in the nucleosynthesis predictions with respect to previous AGB models, so that, above $A \simeq 85$, only abundances of *s*-processed isotopes depending on $N(n)$ differ from the published predictions of thermally pulsing LMS models (details are presented in Straniero et al. 1995b). In particular, the new model of *s*-processing in the interpulse period implies a reduction of the Rb/Sr ratio in the envelope and atmosphere: Rb/Sr ≈ 0.05 is a typical value, in close agreement with the ratio found for the atmospheres of the MS/S and barium giants. This result is so weakly dependent on the assumed mass of ^{13}C available for burning that differences in the Rb/Sr ratio related to this parameter would be unmeasurable. Models in which $^{13}C(\alpha, n)^{16}O$ is run in the interpulse period predict similar isotopic Zr abundances to models in which $^{13}C(\alpha, n)^{16}O$ is restricted to the convective thermal pulse. This is to be expected because in neither case does the neutron density attain a value close to the critical density of the ^{95}Zr branch. Hence, the observed isotopic Zr abundances are in good agreement with the predictions for LMS models independently of when $^{13}C(\alpha, n)^{16}O$ runs.

This survey of predicted Rb/Sr and $^{96}Zr/Zr$ ratios for IMS and LMS models shows that IMS models cannot account for the observations. LMS models predict $^{96}Zr/Zr$ ratios below the upper limit provided from our observations. LMS models in which the *s*-process runs during the thermal pulses experienced by the He shell predict a Rb/Sr ratio larger by a factor of 2 to 4 than observed for the barium giants. This discrepancy is entirely removed by the discovery that the *s*-process runs in the interpulse interval when the He shell is radiative.

6. CONCLUDING REMARKS

The Rb abundances reported earlier for barium giants and here for a sample of extrinsic and intrinsic MS/S stars show that the *s*-processed material in these stars was synthesized at such a low neutron density that the unstable nuclide ^{85}Kr decayed rather than undergo a neutron capture. The required low neutron densities are, as we have discussed, in conflict with the high values reported for models of thermal pulses in the He shell of intermediate-mass stars. Our observations of the Zr isotopes are also in conflict with predicted abundances unless the intermediate-mass AGB star has a C-O core mass of less than about 1 $M_\odot$. The conclusion that low-mass rather than intermediate-mass AGB stars comprise the sample of analyzed stars is supported by other observational evidence (Lambert 1991); for example, the high ^{25}Mg and ^{26}Mg abundances expected from operation of the $^{22}Ne(\alpha, n)^{25}Mg$ neutron source in intermediate-mass AGB stars are not observed in some of the considered sample and in other *s*-process enriched stars.

Until recently, operation of the *s*-process in low-mass AGB stars was identified with activation of the reaction $^{13}C(\alpha, n)^{16}O$ when the He shell experienced thermal pulses. Now, Straniero et al. (1995a, b) have predicted that low-mass stars (3 $M_\odot$ and solar composition, in their reported calculations) activate the ^{13}C neutron source in the interpulse intervals when the He shell is radiative rather than convective as in a thermal pulse. Such activation results in significantly lower neutron densities affecting synthesis of nuclides influenced by the ^{85}Kr and ^{95}Zr branchings. Our observations of ^{96}Zr are consistent with all predictions for low-mass AGB stars. The observed Rb abundances, however, are less than those predicted for the *s*-process by thermal pulses in low-mass AGB stars but fully consistent with operation of the *s*-process in the interpulse intervals. Presently, investigation of the *s*-process in interpulse intervals has been restricted to a single model. Our observations would seem to indicate that it is a common occurrence among low-mass AGB stars.

A possibly disquieting fact remains to be faced by advocates of the exclusive role of the LMS models in synthesizing the "main" *s*-process. We refer to the fact that the intrinsic S star HR 8714 is Li rich (relative to other MS/S stars). Although HR 8714 is not a super Li-rich S star like T Sgr, it would seem that

synthesis of lithium by an AGB star is needed to account for HR 8714's Li abundance. Since technetium is present in its atmosphere, we suppose it to be an intrinsic S star. Sackmann & Boothroyd (1992) calculations of lithium synthesis by luminous S stars with a hot-bottom convective envelope (HBCE) show that lithium is produced in IMS but not LMS stars. Comparison of the predicted and observed Rb abundances and the Mg isotopic ratios, however, suggests that HR 8714 is a LMS star. Our spectra of T Sgr, the super Li-rich star, suggest ^{96}Zr is not abundant. Unfortunately, the star's Rb abundance is as yet unknown (and probably unknowable). The Sackmann & Boothroyd (1992) models predict Li is synthesized by luminous AGB stars of mass 4–6 $M_{\odot}$. Boothroyd & Sackmann (1992) predict core masses of 0.85 to 0.96 $M_{\odot}$ for such luminous stars having an initial solar composition. As noted in § 5.2, Malaney's (1986) predictions show the excess of ^{96}Zr to occur for core masses greater than about 1 $M_{\odot}$. Thus, it seems that the presence of Li and the absence of ^{96}Zr are compatible with the available AGB models. One expects, however, T Sgr to be rich in Rb. It may be worthwhile to search for nonresonance lines of Rb I.

Since production of Li by a HBCE is seemingly sensitive to details of the stellar structure calculations, we suppose it may be possible to reconcile Li production with a star's status as a LMS. We note in this context that there is evidence of lithium production in Magellanic cloud stars at luminosities fainter than predicted by Sackmann and Boothroyd (Smith et al. 1995). It is not clear that these fainter stars are LMS but they do suggest that more remains to be learned about lithium production in AGB stars.

Completion of the story of Rb, and the *s*-process, in AGB stars will surely require additional observations. The CH star, the metal-poor breed of barium giants, are deserving of attention because as expected and observed the neutron exposures experienced by these stars is considerably higher than for the barium giants (Vanture 1992). Furthermore, the neutron density is expected to increase with decreasing metallicity (Clayton 1988; Busso et al. 1995). Apart from the Sun, nothing is known about Rb in main-sequence stars as a function of metallicity. As noted above, the Sun seems to be unusual with respect to Rb: the Rb/Sr ratio for the solar main component which is attributed to AGB stars is a factor of about 3 larger than that found for the Ba and MS/S stars; there is a suspicion that the solar Rb abundance is slightly higher than found in the K and M giants. For these and other stronger reasons it would be of interest to investigate the run of Rb abundance with metallicity in main-sequence stars: the Rb I lines at 7800 and 7947 Å will be detectable in stars of solar and cooler effective temperatures. These studies should be accompanied by an investigation of the non-LTE effects on this trace alkali atom with a low first ionization potential.

We thank J. Tomkin for obtaining some of the spectra used in this study, J. G. Phillips and S. P. Davis for providing lists of TiO and ZrO lines, H. Beer for sending details of his nucleosynthesis calculations, and R. A. Bell for a tape of TiO lines. Research into stellar compositions at the University of Texas is supported in part by the R. A. Welch Foundation and the National Science Foundation (grant AST 93-15124).

REFERENCES

Anders, E., & Grevesse, N. 1989, Geochim. Cosmochim. Acta, 53, 197
Bazan, G., & Lattanzio, J. C. 1993, ApJ, 409, 762
Becker, S. A. 1981, in Physical Processes in Red Giants, ed. I. Iben, Jr. & A. Renzini (Dordrecht: Reidel), 141
Beer, H. 1991, ApJ, 375, 823
Beer, H., & Macklin, R. L. 1989, ApJ, 339, 962
Beer, H., Rupp, G., Voss, F., & Käppeler, F. 1991, ApJ, 379, 420
Beer, H., Voss, F., & Winters, R. R. 1992, ApJS, 80, 403
Bell, R. A., Dwivedi, P. H., Branch, D., & Huffaker, J. N. 1979, ApJS, 41, 593
Blöcker, T., & Schönberner, D. 1995, Nuclei in the Cosmos III, ed. M. Busso, R. Gallino, & C. M. Raiteri (New York: AIP), 399
Boothroyd, A. I., & Sackmann, I.-J. 1992, ApJ, 393, L21
Brown, J. A., Smith, V. V., Lambert, D. L., Dutchover, E. Jr., Hinkle, K. H., & Johnson, H. R. 1990, AJ, 99. 1930
Burbidge, E. M., Burbidge, G. R., Fowler, W. A., & Hoyle, F. 1957, Rev. Mod. Phys.,29, 547
Busso, M., Gallino, R., Lambert, D. L., Raiteri, C. M., & Smith, V. V. 1992, ApJ, 399, 218
Busso, M., Lambert, D. L., Beglio, L., Gallino, R., Raiteri, C. M., & Smith, V. V. 1995, ApJ, 446 in press
Busso, M., Picchio, G., Gallino, R., & Chieffi, A. 1988, ApJ, 326, 196
Clayton, D. D. 1988, MNRAS, 234
Clegg, R. E. S., Lambert, D. L., & Bell, R. A. 1979, ApJ, 234, 188
Davis, S. P., Littleton, J. E., & Phillips, J. G. 1986, ApJ, 309, 339
Davis, S. P., & Phillips, J. G. 1963, The Red System ($A^2\Pi$–$X^2\Sigma$) of the CN Molecule (Berkeley: Univ. California Press)
Doverstål, M., & Weijnitz, P. 1992, Molec. Phys. 75, 1375
Edvardsson, B., Andersen, J., Gustafsson, B., Lambert, D. L., Nissen, P. E., & Tomkin, J. 1993, A&A, 275, 101
Feinberg, J., & Davis, S. P. 1977, J. Molec. Spectrosc., 69, 445
Gallino, R. 1989, in The Evolution of Peculiar Red Giants, ed. H. R. Johnson & B. Zuckerman (Cambridge: Cambridge Univ. Press), 176
Grevesse, N. 1984, Phys. Scripta, T8, 49
Hammer, P. D., & Davis, S. P. 1980, ApJ, 237, L51
Hauge, O. 1972, Solar Phys., 26, 263
Hollowell, D., & Iben, I., Jr. 1988, ApJ, 333, L25
———. 1989, ApJ, 340, 966
Holweger, H., & Müller, E. A. 1974, Solar Phys., 39, 19
Iben, I., Jr. 1991, in Evolution of Stars: The Photospheric Abundance Connection, ed. G. Michaud & A. Tutukov (Dordrecht: Kluwer), 257
Iben, I., Jr., & Renzini, A. 1983a, ApJ, 259, L79
———. 1982b, ApJ, 263, L23
Iben, I., Jr., & Renzini, A. 1983, ARA&A, 21, 271
Jorissen, A., Frayer, D. T., Johnson, H. R., Mayor, M., & Smith, V. V. 1993, A&A, 271, 463
Käppeler, F., Beer, H., & Wisshak, K. 1989, Rep. Prog. Phys., 52, 945
Käppeler, F., Gallion, R., Busso, M., Picchio, G., & Raiteri, C. M. 1990, ApJ, 354, 630
Käppeler, F., et al. 1994, ApJ, 437, 396
Kovács, N. 1983, A&A, 120, 21
Kurucz, R. L., & Peytremann, E. 1975, Smithsonian Astrophys. Obs. Spec. Rep. 362
Lambert, D. L. 1988, in The Impact of Very High S/N Spectroscopy on Stellar Physics, ed. G. Cayrel de Strobel & M. Spite (Dordrecht: Kluwer), 563
———. 1991, in Evolution of Stars: The Photospheric Abundance Connection, ed. G. Michaud & A. Tutukov (Dordrecht: Kluwer), 299
Lambert, D. L., & Luck, R. E. 1976, Observatory, 96, 100
Lambert, D. L., & Mallia, E. A. 1968, MNRAS, 140, 13
Larsson, M. 1983, A&A, 128, 291
Little, S. J., Little-Marenin, I. R., & Bauer, W. H. 1987, AJ, 94, 985
Littleton, J. E., & Davis, S. P. 1985, ApJ, 296, 152
Luck, R. E., & Bond, H. E. 1991, ApJS, 77, 515
Luck, R. E., & Lambert, D. L. 1977, ApJ, 211, 443
———. 1982, ApJ, 256, 189
Malaney, R. A. 1986, in Advances in Nuclear Astrophysics, ed. E. Vangioni-Flam et al. (Gif-sur-Yvette: Editions Frontières), 407
———. 1987, ApJ, 321, 832
Malaney, R. A., & Lambert, D. L. 1988, MNRAS, 235, 695
Merrill, P. M. 1952, ApJ, 116, 21
Nagai, Y., Igashira, M., Takeda, K., Mukai, N., Motoyama, S., Uesawa, F., Kitazawa, H., & Fukuda, T. 1991, ApJ, 372, 683
North, P., Berthet, S., & Lanz, T. 1994, A&A, 281, 775
Pedley, J. B., & Marshall, R. M. 1983, J. Phys. Chem. Ref. Data, 12, 967
Peery, B. F., & Beebe, R. F. 1970, ApJ, 160, 619
Phillips, J. G. 1973, ApJS, 26, 313
Phillips, J. G., & Davis, S. P. 1976, ApJS, 32, 537
———. 1979, ApJ, 229, 867
Plez, B., Smith, V. V., & Lambert, D. L. 1993, ApJ, 418, 812
Raiteri, C. M., Gallino, R., Busso, M., Neuberger, D., & Käppeler, F. 1993, ApJ, 419, 207
Sackmann, I.-J., & Boothroyd, A. 1991, in Evolution of Stars: The Photospheric Abundance Connection, ed. G. Michaud & A. Tutukov (Dordrecht: Kluwer), 275
Sackmann, I.-J., & Boothroyd, A. 1992, ApJ, 392, L71

Schadee, A., & Davis, D. N. 1968, ApJ, 152, 169
Smith, V. V. 1984, A&A, 326
Smith, V. V., & Lambert, D. L. 1984, PASP, 96, 226
———. 1985, ApJ, 294, 326
———. 1986, ApJ, 311, 843
———. 1990, ApJS, 72, 387
Smith, V. V., Plez, B., Lambert, D. L., & Lubowich, D. 1995, ApJ, 441, 735
Sneden, C. 1973, Ph.D. thesis, Univ. Texas
Straniero, O., Gallino, R., Busso, M., Chieffi, A., Raiteri, C. M., Salaris, M., & Limongi, M. 1995a, in Nuclei in the Cosmos III, ed. M. Busso, R. Gallino, & C. M. Raiteri (New York: AIP), 407
Straniero, O., Gallino, R., Busso, M., Chieffi, A., Raiteri, C. M., Limongi, M., & Salaris, M. 1995b, ApJ, 440, L85
Takahashi, K., & Yokoi, K. 1987, Atomic Data Nucl. Data Tables, 36, 375
Tatum, J. B. 1978, MNRAS, 141, 459
Tatum, J. B., & Sauval, J. 1984, ApJS, 56, 193
Tomkin, J., & Lambert, D. L. 1983, ApJ, 273, 722
———. 1986, ApJ, 311, 819
Toukan, K. A., & Käppeler, F. 1990, ApJ, 348, 357
Tsuji, T. 1971, PASJ, 23, 275
———. 1973, A&A, 23, 411
Vanture, A. D. 1992, AJ, 104, 1997
Wallerstein, G. 1992, PASP, 104, 511
Ward, R. A. 1977, ApJ, 216, 540
Ward, R. A., & Newman, M. J. 1978, ApJ, 219, 195
Ward, R. A., Newman, M. J., & Clayton, D. D. 1976, ApJS, 31, 33
Whiting, E. E. 1972, NASA Tech. Note, D-7268
Woolf, V., Tomkin, J., & Lambert, D. L. 1995, ApJ, in press
Zook, A. C. 1978, ApJ, 213, L113
———. 1985, ApJ, 289, 356